Science Advances
AAAS

advances.sciencemag.org/cgi/content/full/7/5/eabe5504/DC1

Supplementary Materials for

Complexes of the neurotensin receptor 1 with small-molecule ligands reveal structural determinants of full, partial, and inverse agonism

Mattia Deluigi, Alexander Klipp, Christoph Klenk, Lisa Merklinger, Stefanie A. Eberle, Lena Morstein, Philipp Heine, Peer R. E. Mittl, Patrick Ernst, Theodore M. Kamenecka, Yuanjun He, Santiago Vacca, Pascal Egloff, Annemarie Honegger, Andreas Plückthun*

*Corresponding author. Email: plueckthun@bioc.uzh.ch

Published 27 January 2021, *Sci. Adv.* **7**, eabe5504 (2021)
DOI: 10.1126/sciadv.abe5504

This PDF file includes:

Figs. S1 to S16
Tables S1 to S12
Note S1
Supplementary materials and methods
References

Supplementary figures

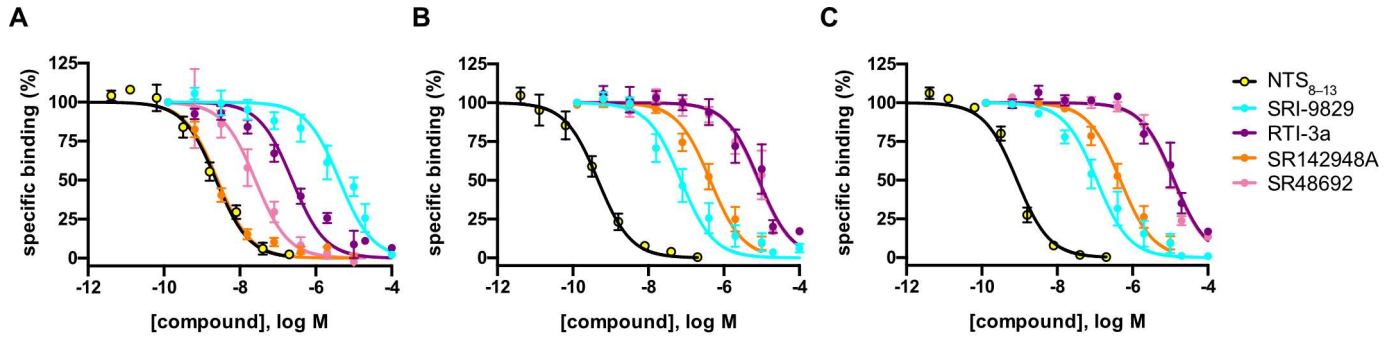

Fig. S1. Ligand-binding to wild-type rNTSR1, NTSR1-H4$_X$, and NTSR1-H4$_X^{\Delta D12}$. (**A–C**) Competition ligand binding of HL488-NTS$_{8–13}$ with ligands used for crystallization. Binding was measured in membranes from cells expressing (**A**) wild-type rNTSR1, (**B**) the crystallized receptor variant with DARPin (NTSR1-H4$_X$) or (**C**) without DARPin fusion (NTSR1-H4$_X^{\Delta D12}$). Data are shown as mean values ± SEM from 5–9 independent experiments performed in duplicates. Note that due to the ~40-fold increased affinity of the tracer peptide (HL488-NTS$_{8–13}$) for NTSR1-H4 compared to wild-type rNTSR1, the competition curves in panel (A) cannot be directly compared with those in panels (B) and (C). Instead, see K_i values reported in table S2.

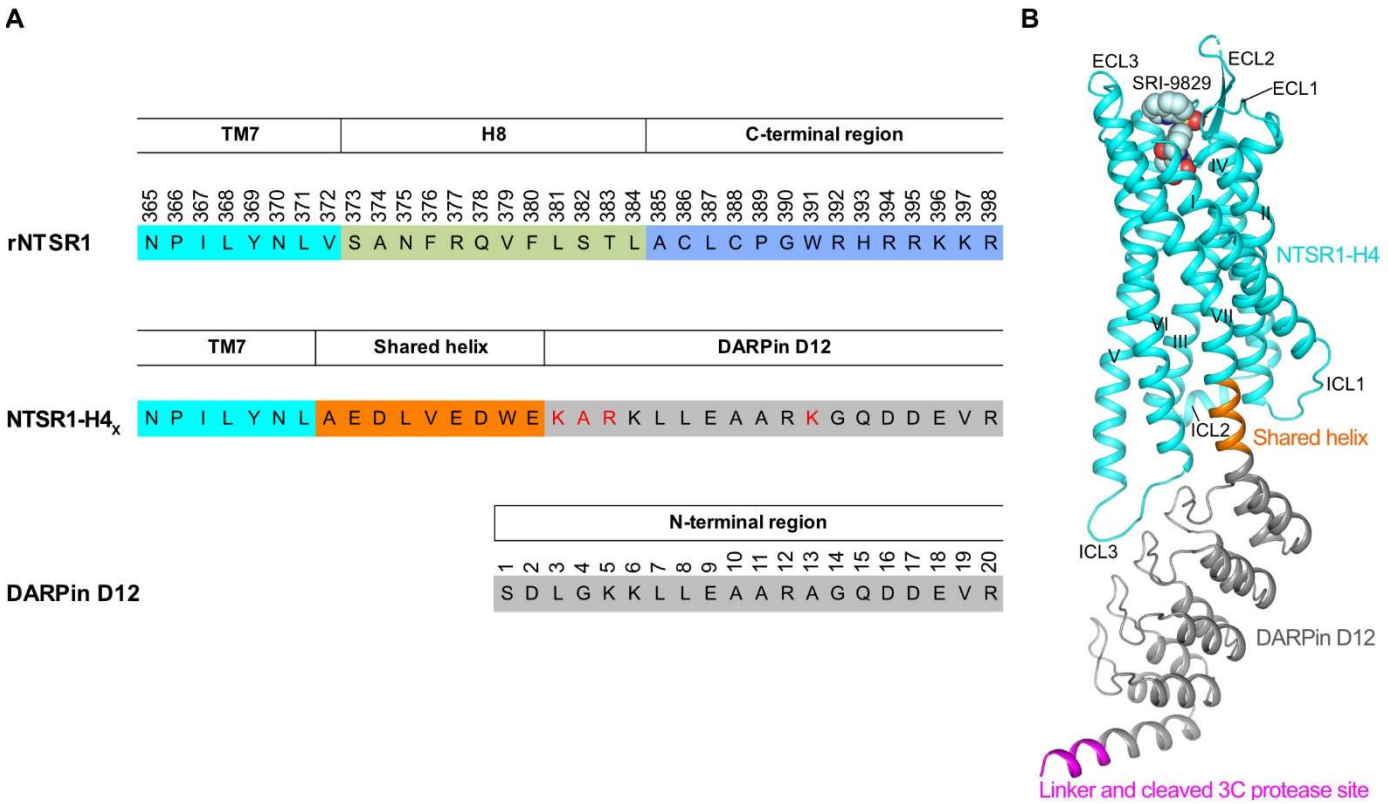

Fig. S2. Overview of the new crystallization chaperone design. (**A**) Fusion site. Top row: C-terminal end of TM7 (cyan), helix 8 (light green) and beginning of C-terminal region (light blue) in rNTSR1. Bottom row: N-terminal region of DARPin D12 (grey). Middle row: crystallized fusion construct NTSR1-H4$_{X.}$ It is a fusion of the C-terminal end of TM7 of rNTSR1 (cyan) via a shared helix (orange) to DARPin D12 (grey). Corresponding parts of the amino acid sequence are aligned to rNTSR1 TM7 in the top row, and to DARPin D12 in the bottom row. The first two residues of the N-terminus of DARPin D12 were omitted, and four point mutations, namely L3K, G4A, K5R and A13K (all colored in red) were introduced. (**B**) Representative overview structure of NTSR1-H4$_X$, here in complex with the orthosteric ligand SRI-9829. The protein is shown in cartoon representation, the ligand SRI-9829 as spheres. NTSR1-H4 is colored cyan, SRI-9829 pale cyan, the shared helix orange, DARPin D12 grey. Of note, the C-terminal region of the crystallized fusion construct, colored magenta, which includes a short linker sequence followed by a cleaved 3C protease site (see Methods), turned out to be partially α-helical and established crystal contacts. ECL: extracellular loop; ICL: intracellular loop.

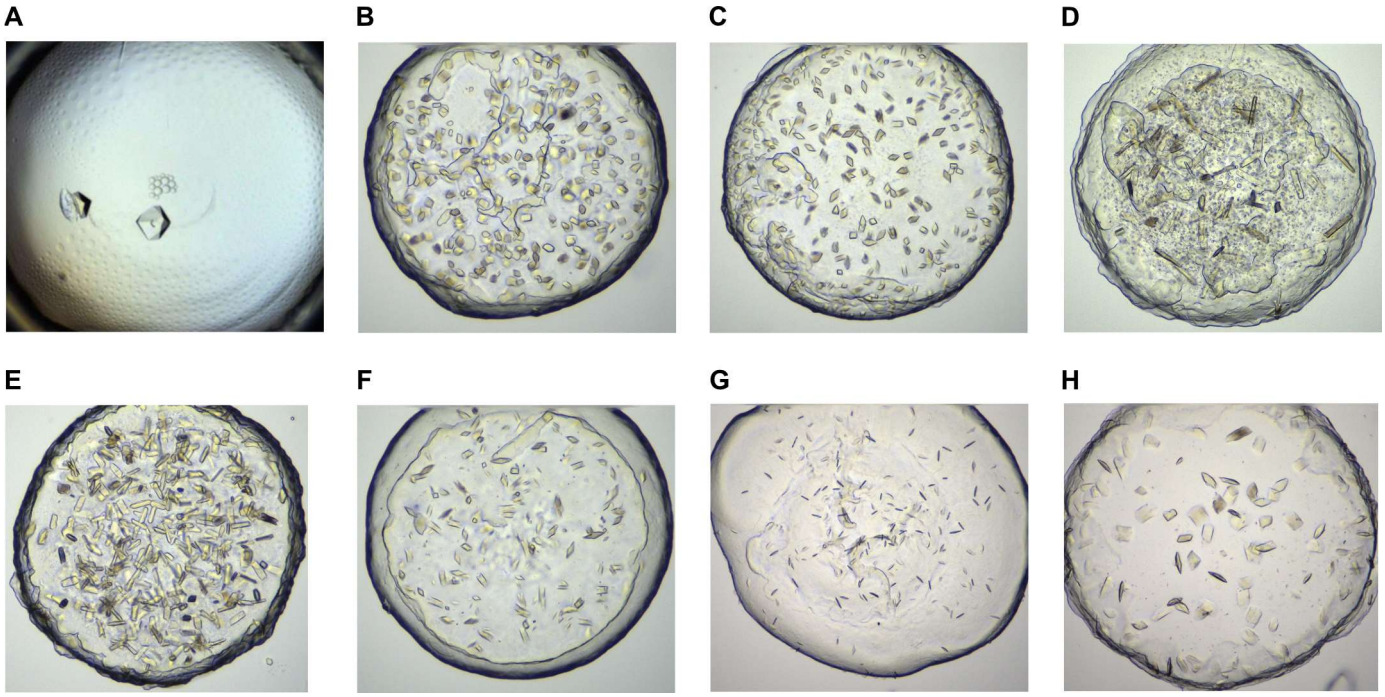

Fig. S3. Representative pictures of crystals obtained in this study. (**A**) Crystals of NTSR1-H4$_X$ grown by vapor diffusion in complex with NTS$_{8–13}$. (**B–F**) Crystals of NTSR1-H4$_X$ grown in lipidic cubic phase (LCP) in complex with (**B**) SRI-9829, (**C**) RTI-3a, (**D**) SR48692, (**E**) SR142948A, and (**F**) in the apo state. (**G, H**) Crystals of NTSR1-H4bm$_X$ grown in LCP in complex with (**G**) SR48692 and (**H**) NTS$_{8–13}$. Photo Credit: Mattia Deluigi using a Rock Imager 1000 (Formulatrix), Department of Biochemistry, University of Zurich.

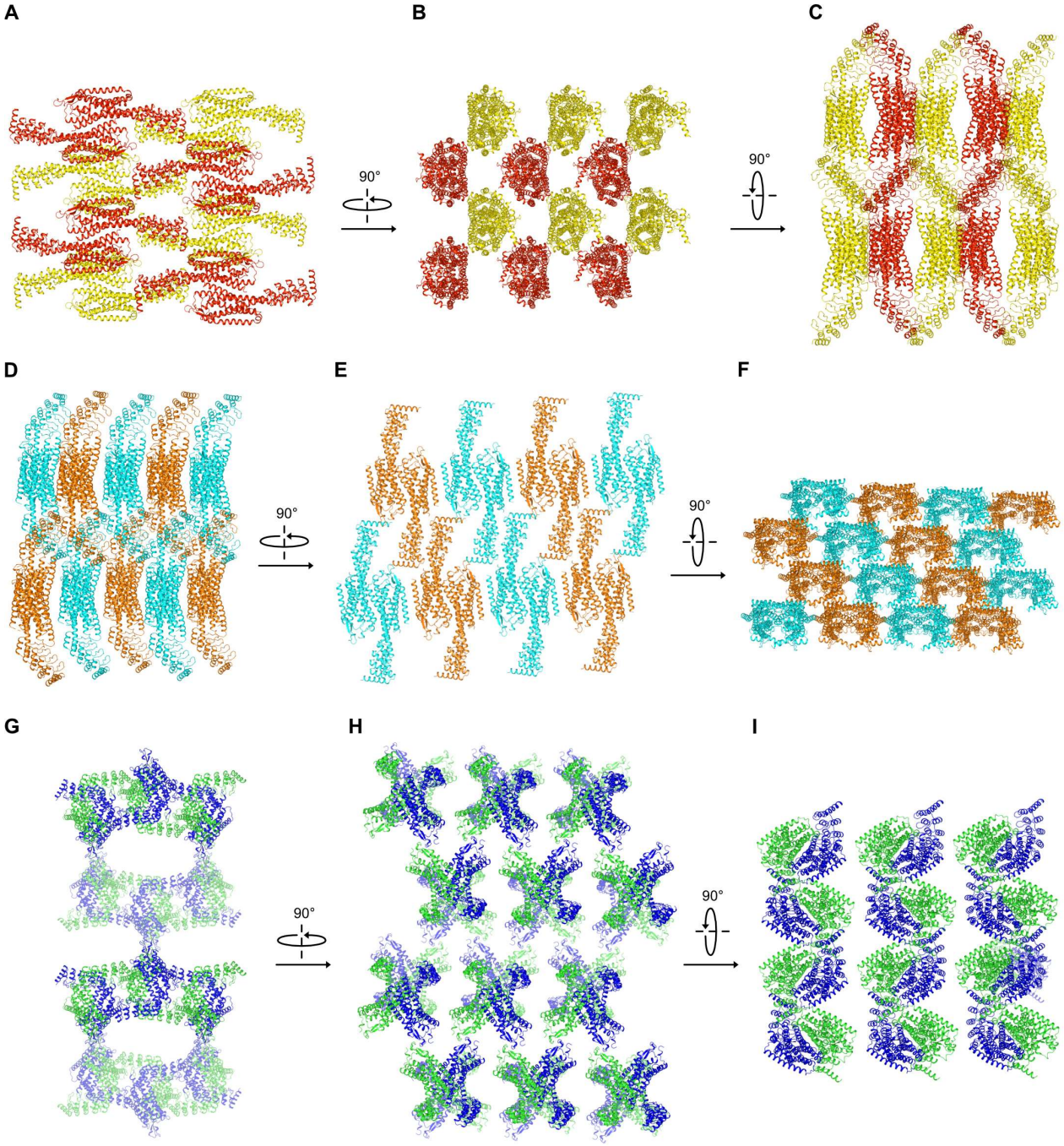

Fig. S4. Examples of crystal packing for crystals obtained by LCP and vapor diffusion crystallization. (**A–C**) LCP crystal packing in the space group $C222_1$ viewed along the (**A**) a-axis, (**B**) b-axis, and (**C**) c-axis of the unit cell, where two antiparallel molecules (colored in red and yellow) form a main crystallization interface. (**D–F**) LCP crystal packing in the space group C121 viewed along the (**D**) a-axis, (**E**) b-axis, and (**F**) c-axis of the unit cell, where two antiparallel molecules (colored in cyan and orange) form a main crystallization interface. (**G–I**) Vapor diffusion crystal packing in the space group $P2_12_12_1$ viewed along the (**G**) a-axis, (**H**) b-axis, and (**I**) c-axis of the unit cell, where two molecules (colored in green and blue) form a main crystallization interface. Molecules lying in the back plane are displayed transparent. Ligands have been omitted for clarity.

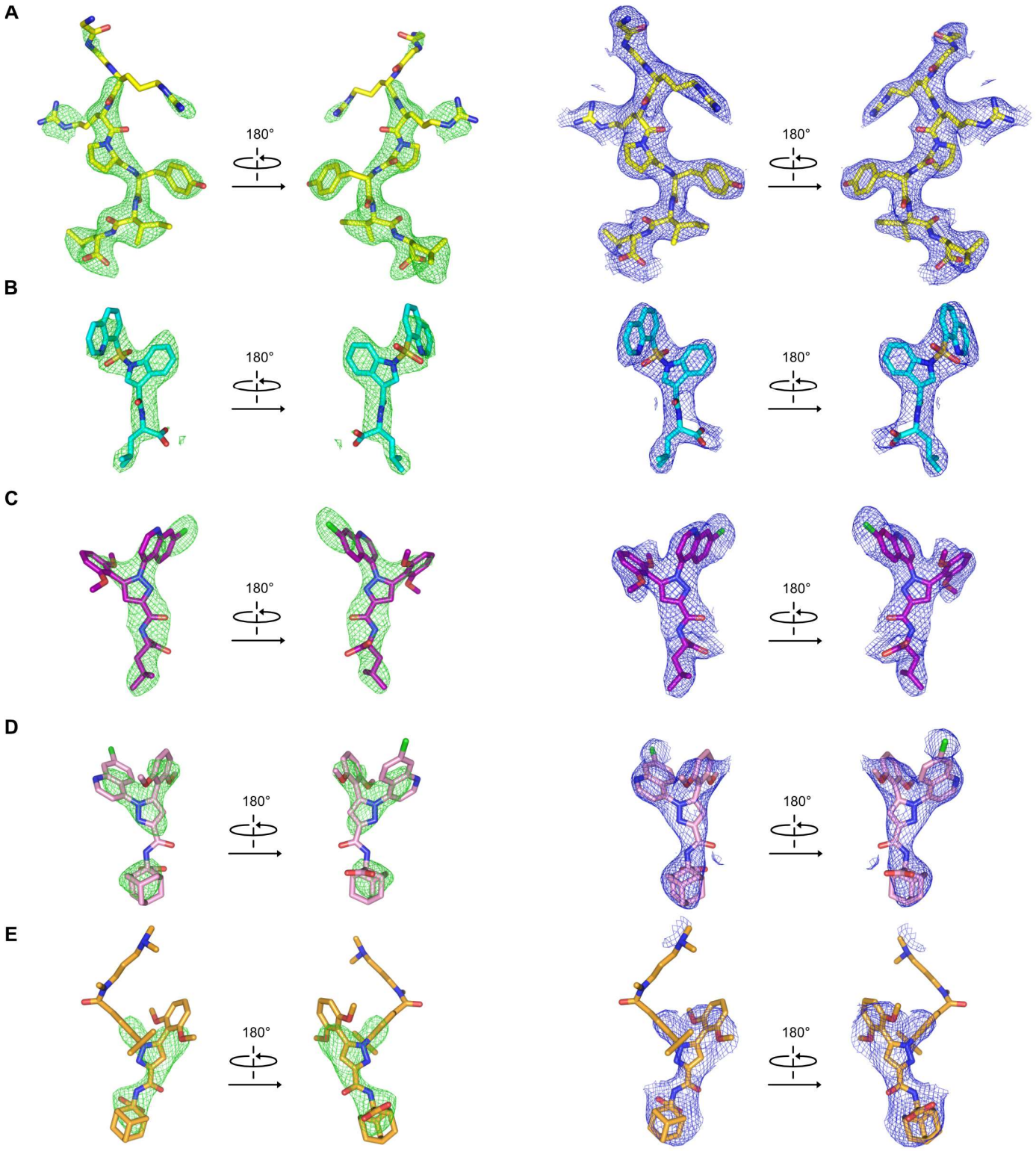

Fig. S5. Electron density of ligands co-crystallized with NTSR1-H4x. (**A–E**) Electron density of (**A**) $NTS_{8–13}$ (two Gly residues of the co-crystallized ligand, GPGG-$NTS_{8–13}$ (see Methods), are also visible in the density), (**B**) SRI-9829, (**C**) RTI-3a, (**D**) SR48692, and (**E**) SR142948A. $F_o−F_c$ electron density maps are shown in green mesh contoured at 3.0 σ. $2F_o−F_c$ electron density maps are shown in blue mesh contoured at 1.0 σ. Ligands are shown as sticks. All ligands could be unambiguously placed in the electron density.

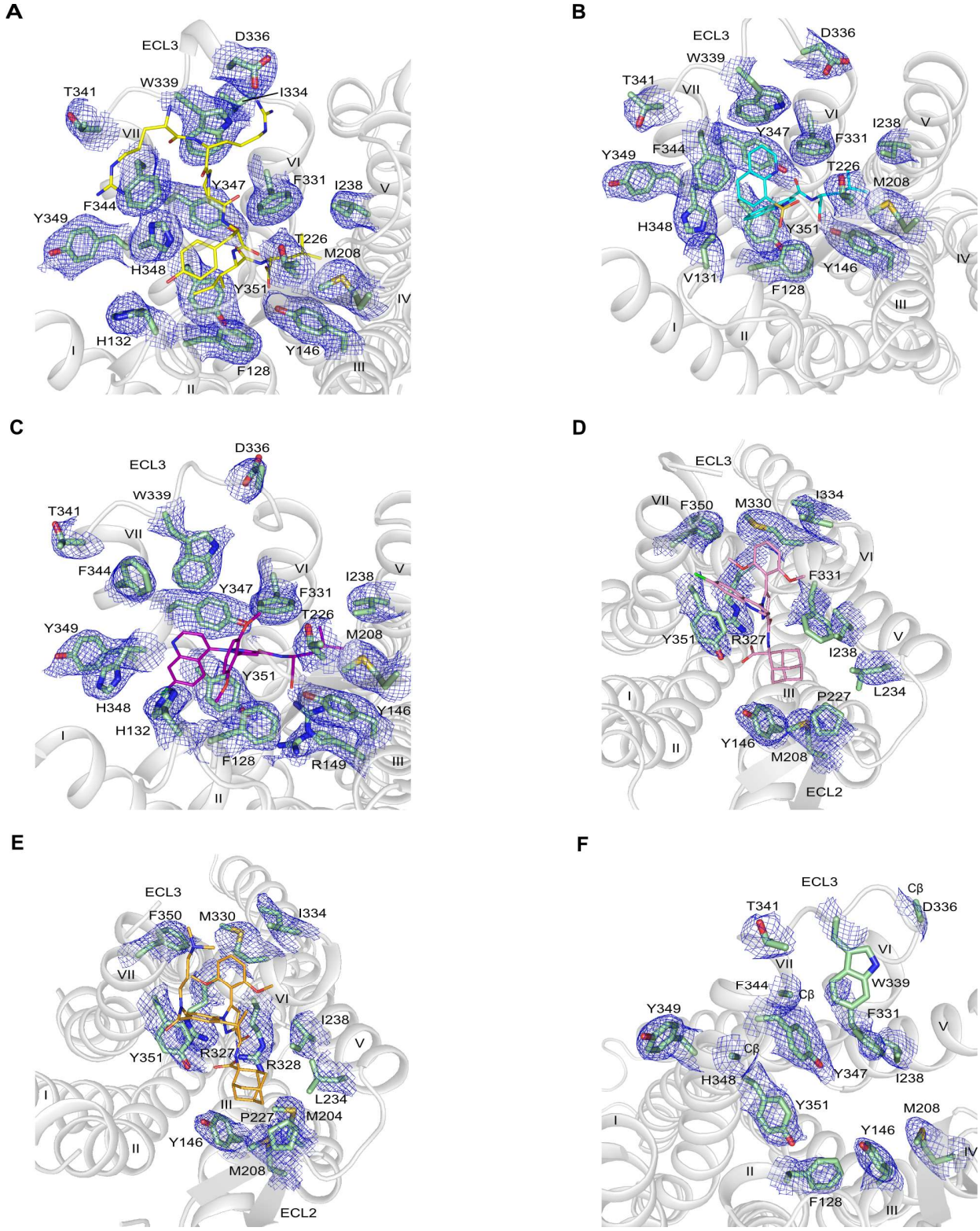

Fig. S6. Electron density in key receptor regions in the structures of NTSR1-H4x. (**A–F**) Electron density in the complexes with (**A**) NTS_{8-13}, (**B**) SRI-9829, (**C**) RTI-3a, (**D**) SR48692, (**E**) SR142948A, and (**F**) for the apo structure. L234 is a mutation of NTSR1-H4 (V in wild-type rNTSR1). The ligands are shown as thin sticks and colored as in fig. S5. $2F_o-F_c$ electron density maps are shown in blue mesh contoured at 1.0 σ. Cβ indicates that the electron density for the remaining part of the side chain is missing.

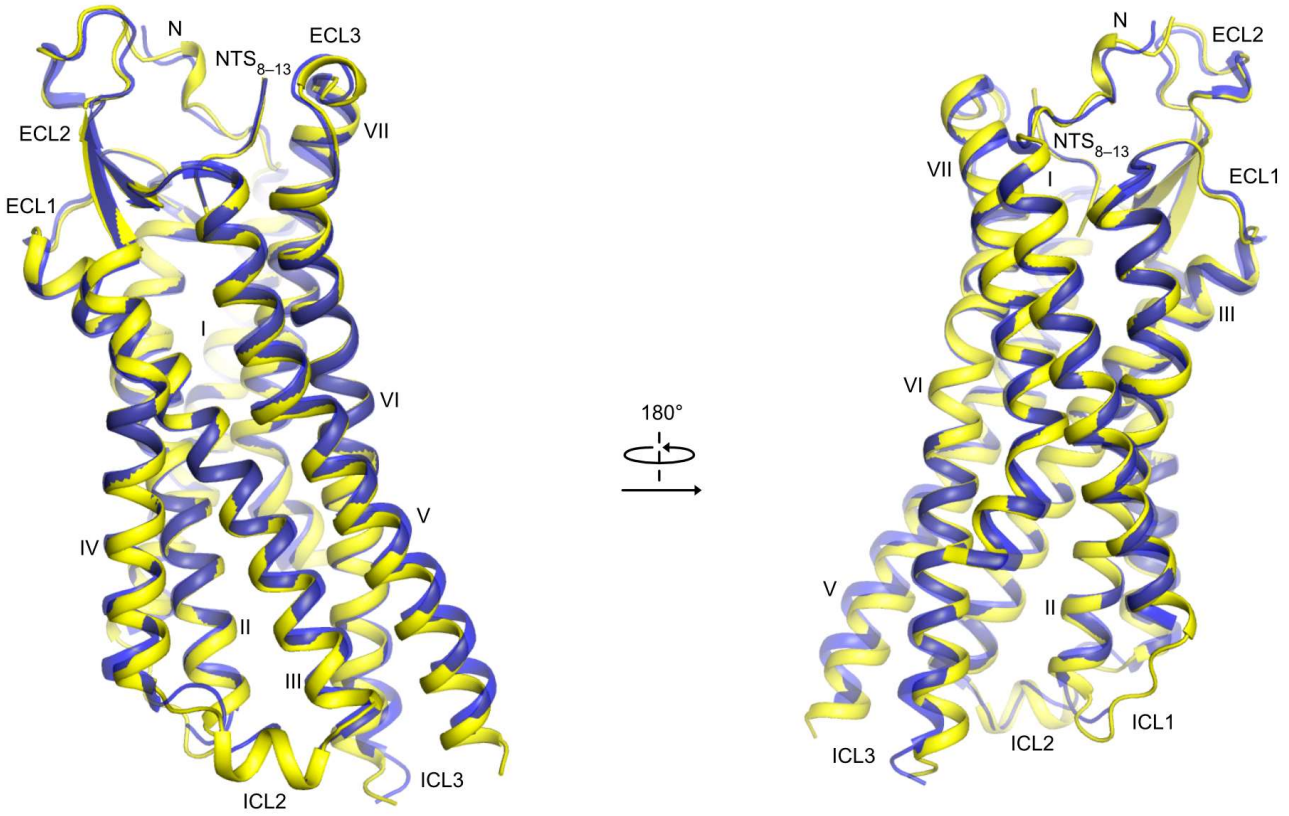

Fig. S7. The fusion of DARPin D12 to the C-terminus of TM7 does not cause significant structural deviations in the 7TM bundle. Superposition of $NTS_{8–13}$-bound NTSR1-H4, either fused to DARPin D12 ($NTSR1\text{-}H4_X$, colored in yellow) or unfused (PDB ID: 4BWB (*9*), colored in blue). The root-mean-squared deviation for Cα atoms ($RMSD_{C\alpha}$) in the 7TM bundle corresponds to only 0.55 Å. The receptor backbone and $NTS_{8–13}$ are depicted in cartoon representation. H8 (in the unfused construct) and the DARPin (in the fused construct) have been omitted for clarity.

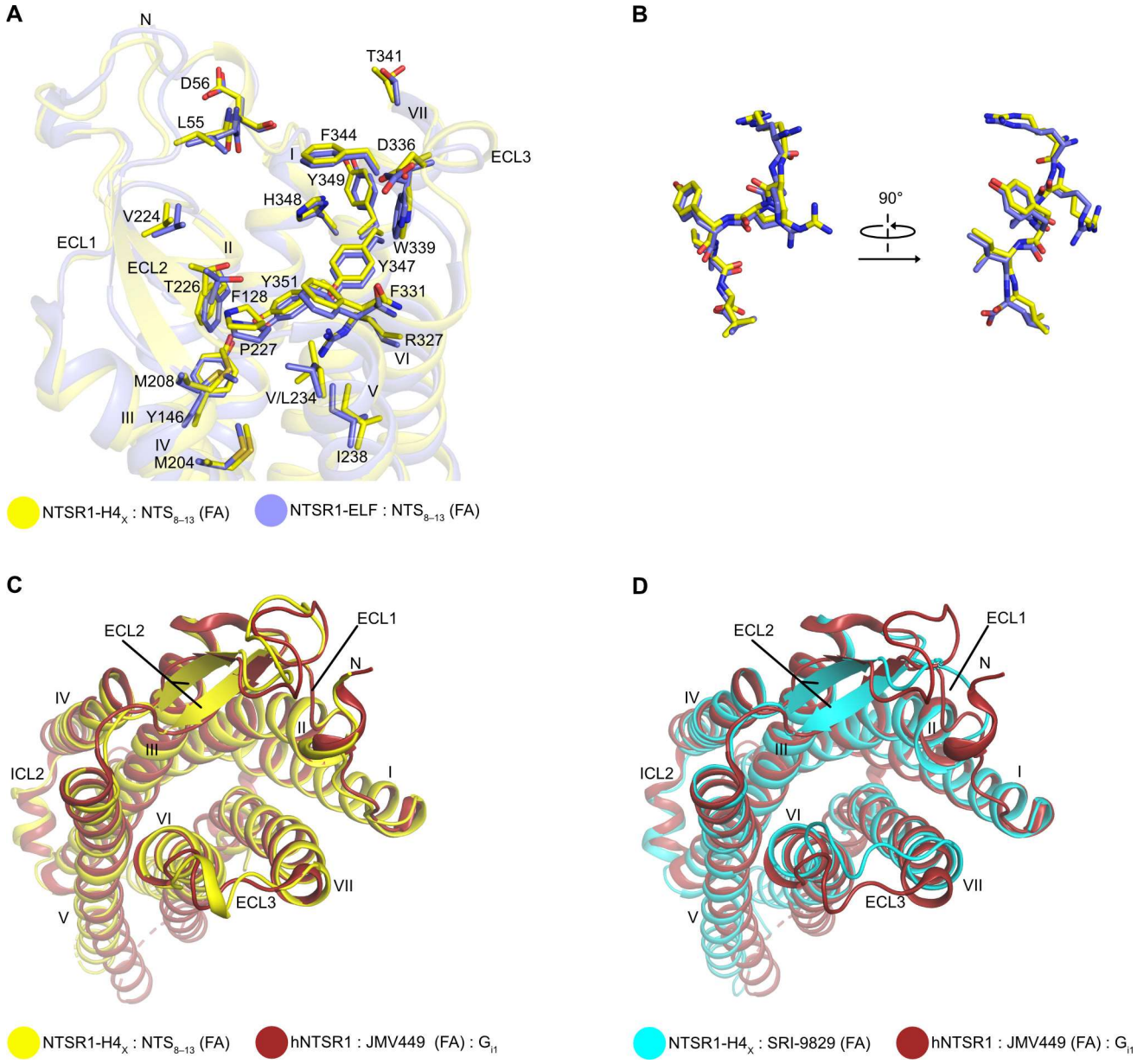

Fig. S8. NTSR1-H4$_X$ bound to full agonists (FA) adopts a virtually identical conformation in the extracellular half as previously reported active-state structures. (**A, B**) Superposition of NTSR1-H4$_X$ with NTSR1-ELF (PDB ID: 4XEE (*10*)), both bound to NTS$_{8–13}$. (**A**) TM I–VII, ECL1–3, and key residues in orthosteric pocket and ECL3, and (**B**) NTS$_{8–13}$ binding mode, as viewed from the membrane plane. In the extracellular half, both structures are virtually identical and exhibit a RMSD$_{C\alpha}$ of only 0.7 Å, including ECL1–3. Additionally, the ligand and the surrounding interacting residues adopt highly similar conformations in both structures. L234 is a mutation of NTSR1-H4 (V in wild-type rNTSR1). The receptor backbone, key residues, and NTS$_{8–13}$ are colored as indicated in the legend. (**C, D**) Superposition of the hNTSR1 : JMV449 (FA) : G$_{i1}$ complex (PDB ID: 6OS9 (*12*)) with NTSR1-H4$_X$ bound to (**C**) NTS$_{8–13}$ (FA) and (**D**) SRI-9829 (FA), viewed from the extracellular side. The ligands, the DARPin, and G$_{i1}$ have been omitted for clarity.

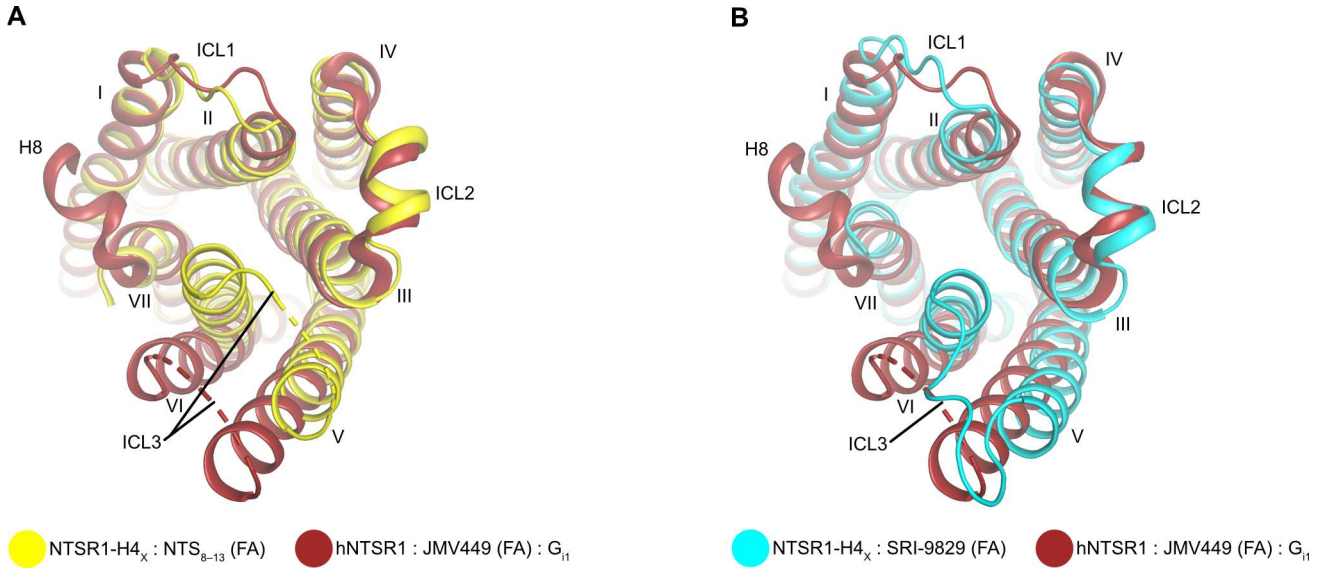

Fig. S9. NTSR1-H4X crystallizes in a signalling-inactive conformation at the intracellular side. (**A, B**) Superposition of the hNTSR1 : JMV449 (FA) : G_{i1} complex (PDB ID: 6OS9 (*12*)) with NTSR1-H4X bound to (**A**) $NTS_{8–13}$ (FA) and (**B**) SRI-9829 (FA), viewed from the intracellular side. FA: Full Agonist. The receptor backbone is depicted in cartoon representation and colored as indicated in the legend. G_{i1}, the DARPin, and the ligands have been omitted for clarity.

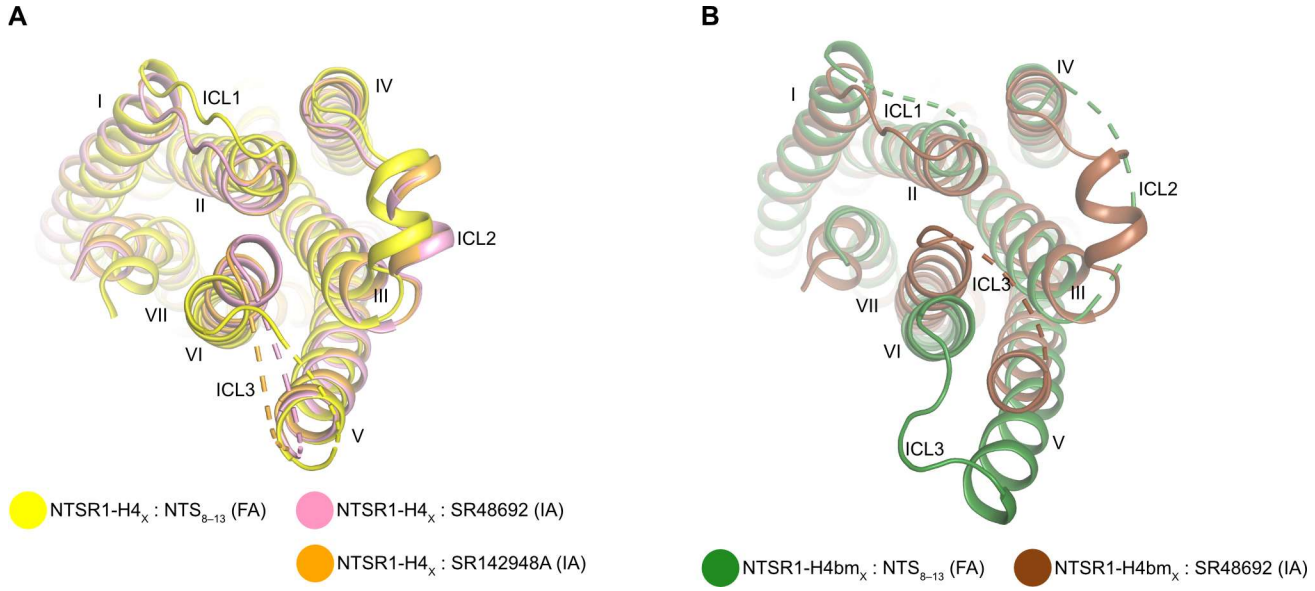

Fig. S10. NTSR1-H4X and NTSR1-H4bmX bound to inverse agonists adopt an apparently fully closed conformation at the intracellular side. (**A**) Superposition of NTSR1-H4$_X$ bound to NTS$_{8–13}$ (FA) with the complexes of SR48692 (IA) and SR142948A (IA), viewed from the intracellular side. (**B**) Superposition of NTSR1-H4bm$_X$ bound to NTS$_{8–13}$ (FA) with the complex of SR48692 (IA), viewed from the intracellular side. FA: Full Agonist; IA: Inverse Agonist. The receptor backbone is depicted in cartoon representation and colored as indicated in the legend. The DARPin and the ligands have been omitted for clarity.

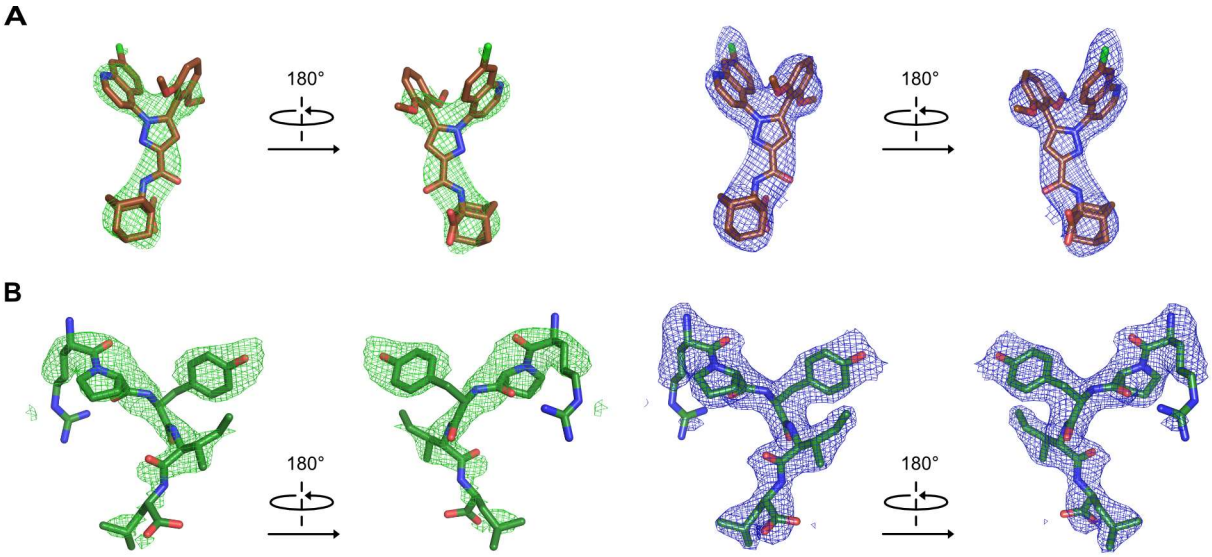

Fig. S11. Electron density of ligands co-crystallized with NTSR1-H4bmx. (**A, B**) Electron density of (**A**) SR48692 and (**B**) $NTS_{8–13}$. Arg_8 of $NTS_{8–13}$ was not modelled as it was not visible in the $F_o–F_c$ electron density map. $F_o–F_c$ electron density maps are shown in green mesh contoured at 2.5 σ. $2F_o–F_c$ electron density maps are shown in blue mesh contoured at 1.0 σ. Ligands are shown as sticks. The protein has been omitted for clarity. Both ligands could be unambiguously placed in the electron density.

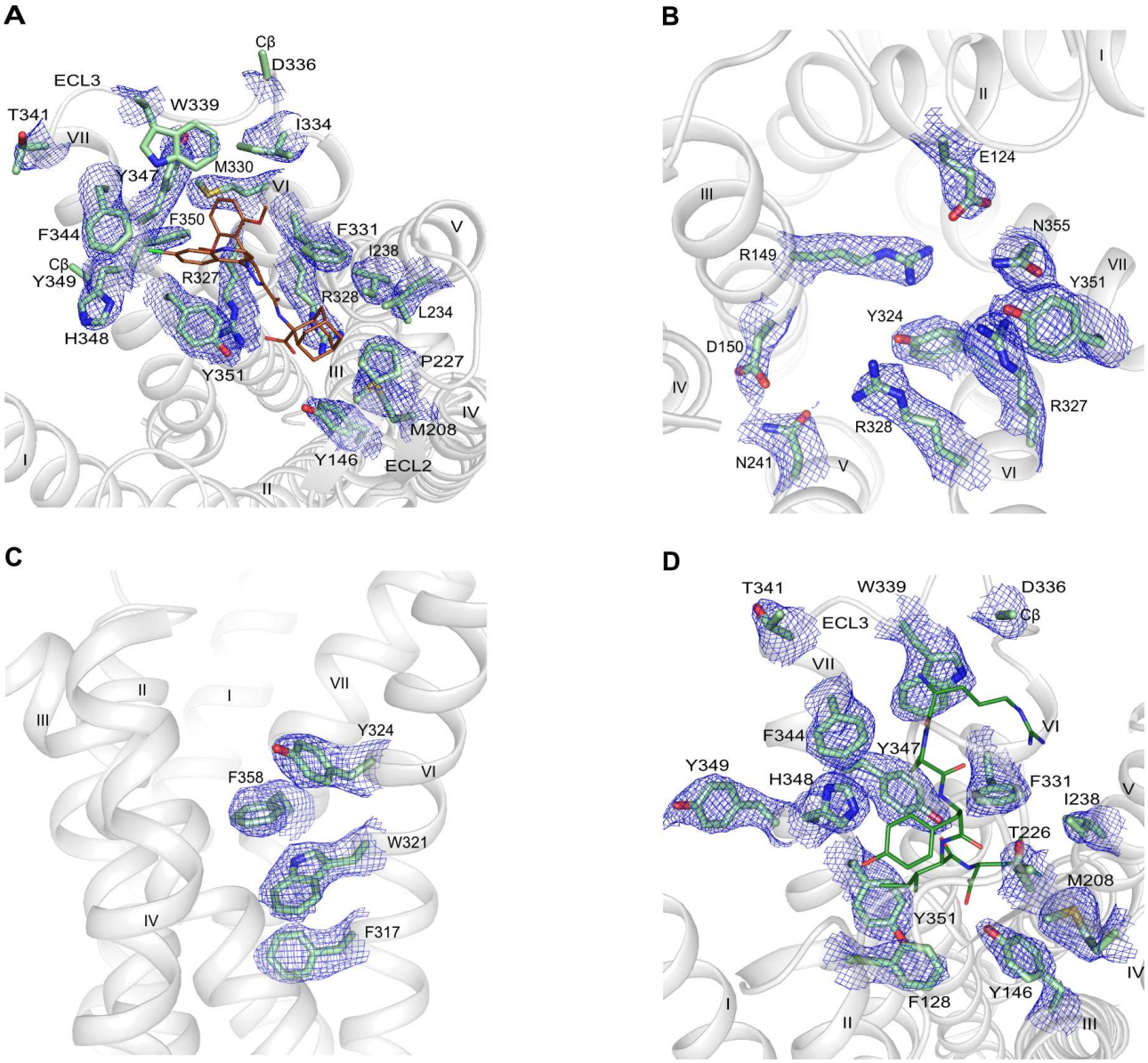

Fig. S12. Electron density in key receptor regions in the structures of NTSR1-H4bm$_X$. (**A–C**) Electron density for the SR48692 complex within (**A**) the orthosteric pocket and ECL3, (**B**) the interhelical polar network, and (**C**) the hydrophobic core. (**D**) Electron density for the NTS$_{8–13}$ complex within the orthosteric pocket and ECL3. The receptor backbone and the side chains are represented as in Fig. 3. L234 is a mutation of NTSR1-H4bm (V in wild-type rNTSR1). The ligands are shown as thin sticks. SR48692 is colored brown, NTS$_{8–13}$ dark green. $2F_o–F_c$ electron density maps are shown in blue mesh contoured at 1.0 σ. Cβ indicates that the electron density for the side chain is missing. The receptor N-terminus and the DARPin have been omitted for clarity. ECL2 has been omitted in panel (B), TM5 in panel (C).

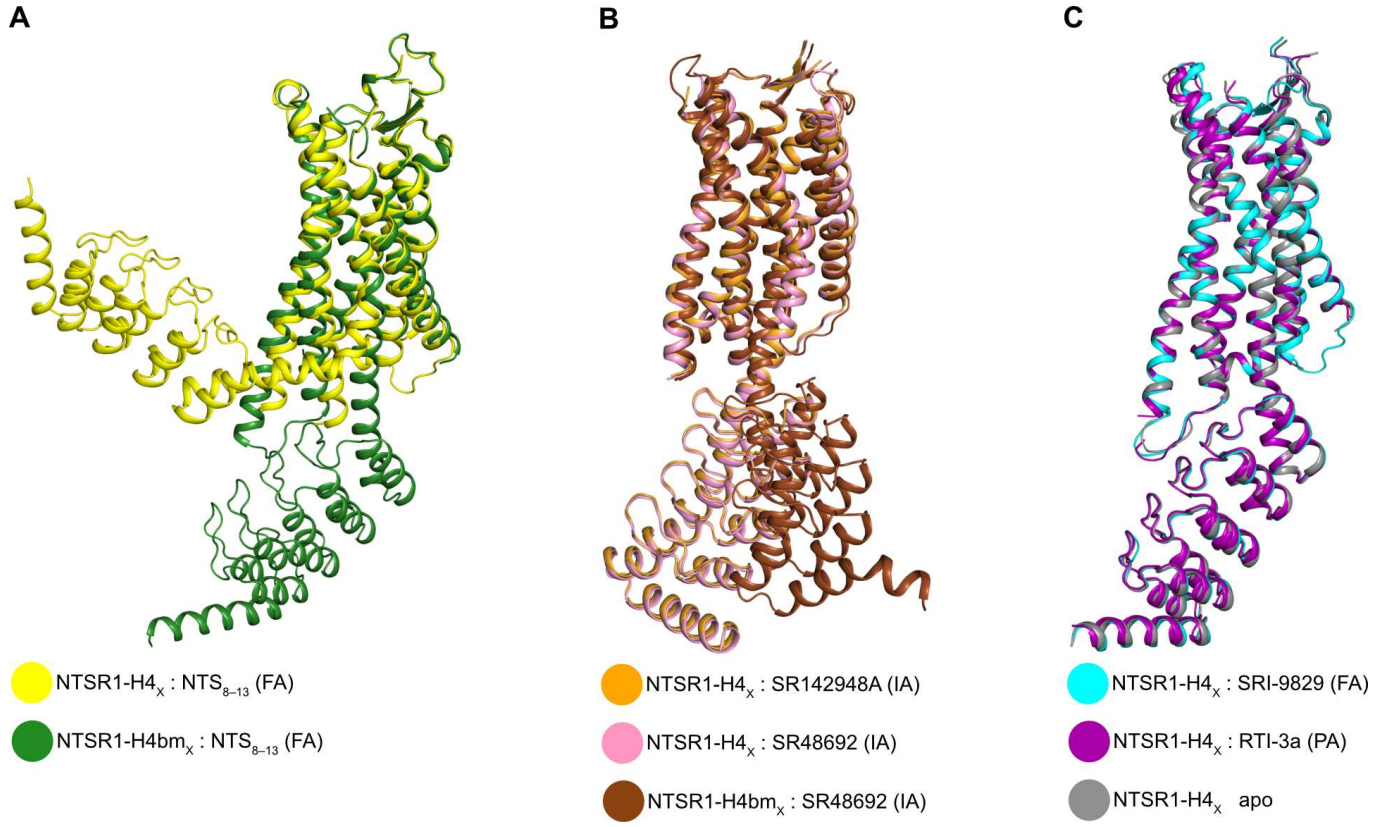

Fig. S13. Ligand-induced conformational changes do not depend on the orientation of the DARPin fusion, the space group or the crystallization method. (**A–C**) Orientation of the DARPin fusion in the complexes of (**A**) NTS$_{8–13}$ (FA), (**B**) SR142948A (IA) and SR48692 (IA), (**C**) SRI-9829 (FA), RTI-3a (PA), and in the apo structure. FA: Full Agonist; PA: Partial Agonist; IA: Inverse Agonist. The GPCR domains were superposed. The ligands have been omitted for clarity. (**A**) The complexes with NTS$_{8–13}$ were solved in the space groups $P2_12_12_1$ (NTSR1-H4$_X$) or C121 (NTSR1-H4bm$_X$), however, their conformation is virtually identical (cf. Fig. 2D). (**B**) The complexes with SR48692 were solved in the space groups C121 (NTSR1-H4$_X$) or $P2_12_12_1$ (NTSR1-H4bm$_X$), but exhibit the same ligand-induced conformational changes (cf. Fig. 2, C and D). The complex of NTSR1-H4$_X$ with SR142948A was solved in the space group C121. (**C**) Finally, the complexes of NTSR1-H4$_X$ with SRI-9829 and RTI-3a, as well as the apo structure, were all solved in the space group $C222_1$, nevertheless they display conformational differences as shown in Fig. 6, B and C. The complex of NTS$_{8–13}$ with NTSR1-H4$_X$ yielded diffraction-quality crystals by vapor diffusion methods, whereas all other structures were obtained from crystals grown in lipidic cubic phase. Crystal contacts (not shown here) were analysed for all structures.

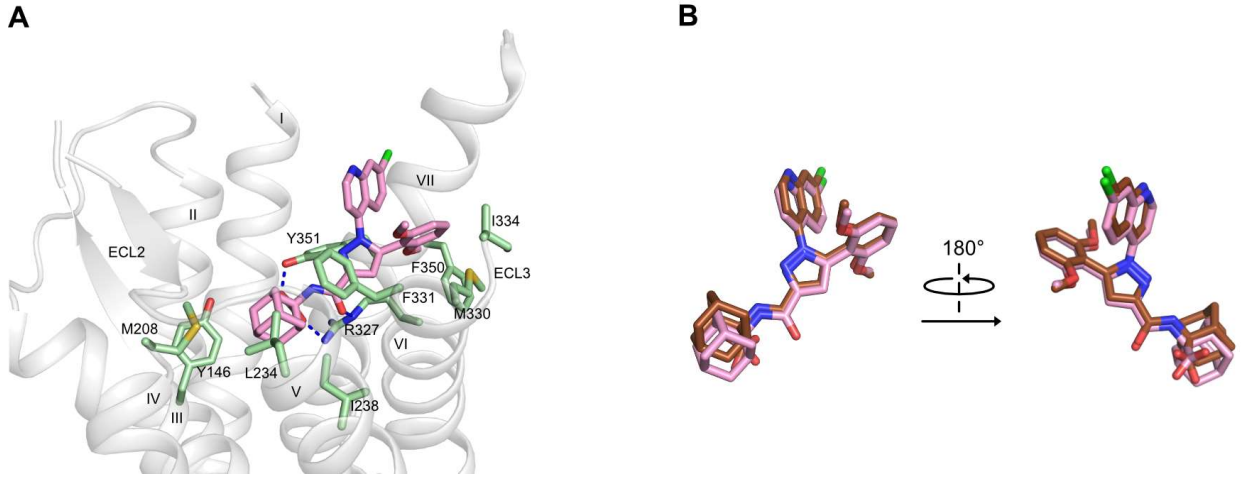

Fig. S14. Binding pocket of SR48692-bound NTSR1-H4$_X$ and superposition of the SR48692 binding mode in the complexes with NTSR1-H4$_X$ and NTSR1-H4bm$_X$. (**A**) Detailed interactions of SR48692 with the receptor, viewed from the extracellular side. The ligand is shown as sticks and is colored pink. Interacting receptor residues are shown as sticks in pale green. L234 is a mutation present in NTSR1-H4 (V in wild-type rNTSR1). The side chains of F344 and Y347, which possibly interact with the ligand, were not well resolved by their electron density and were therefore not modelled. Polar interactions are depicted by dashed blue lines. The DARPin has been omitted for clarity. (**B**) Comparison of the binding mode of SR48692 bound to NTSR1-H4$_X$ and to NTSR1-H4bm$_X$, colored in pink and brown, respectively. After superposition the receptor has been omitted for clarity.

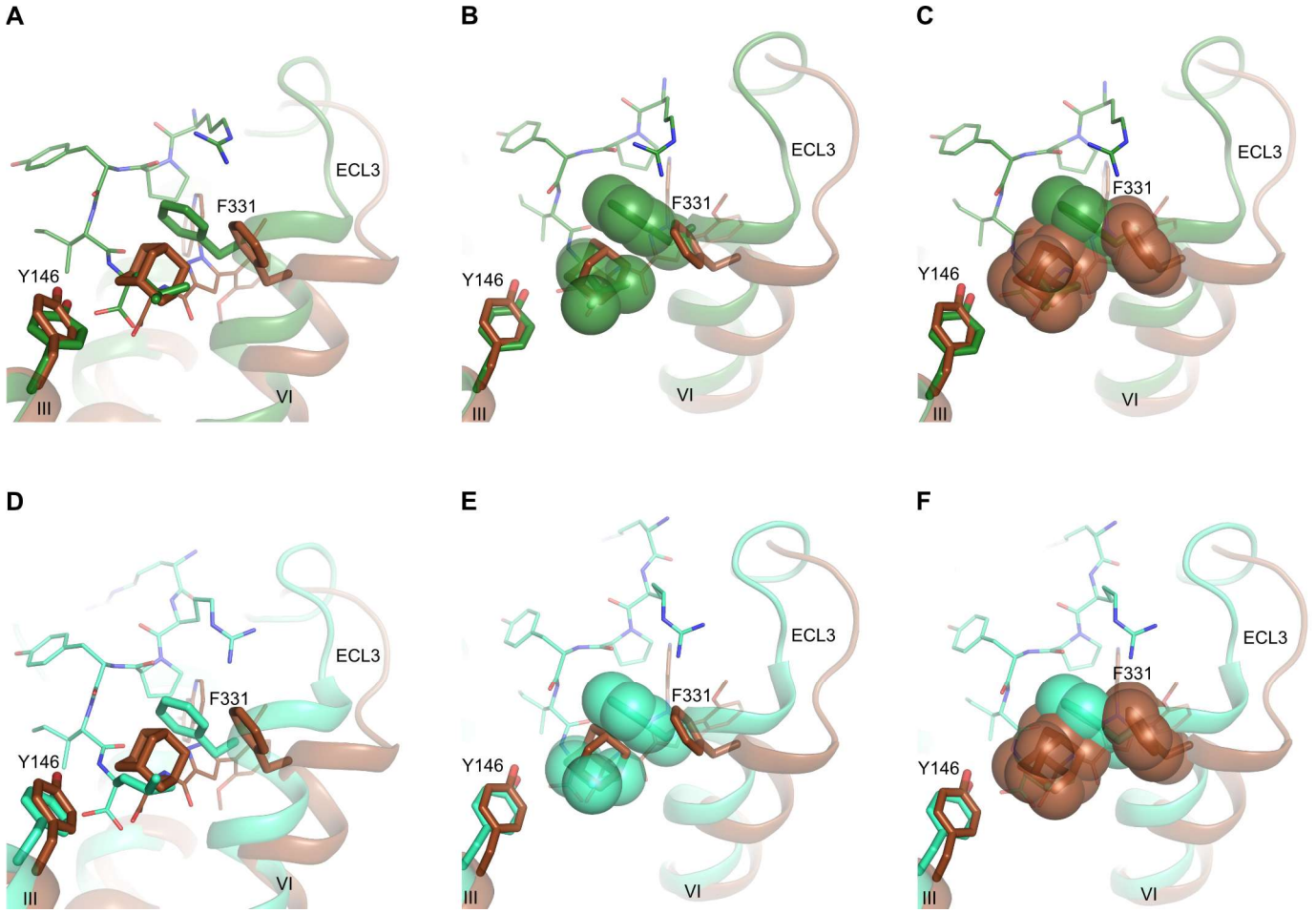

Fig. S15. Steric effects of the isobutyl and adamantyl groups of agonists and inverse agonists, respectively. (**A–C**) Superposition of the $NTS_{8–13}$ (FA) and SR48692 (IA) complexes of NTSR1-H4bm$_X$, showing (**A**) the tilting of TM6 at F331$^{6.58}$ and (**B**) highlighting the space occupied by the isobutyl chain of Leu_{13} and by F331$^{6.58}$ as well as (**C**) the space occupied by the adamantyl moiety and by F331$^{6.58}$, viewed from the membrane plane. FA: Full Agonist; IA: Inverse Agonist. The $NTS_{8–13}$ complex is colored in dark green, the SR48692 complex in brown. (**D–F**) Superposition of the $NTS_{8–13}$ (FA) complex of NTSR1-ELF (PDB ID: 4XEE (*10*)) and the SR48692 (IA) complex of NTSR1-H4bm$_X$, showing (**D**) the tilting of TM6 at F331$^{6.58}$ and (**E**) highlighting the space occupied by the isobutyl chain of Leu_{13} and by F331$^{6.58}$ as well as (**F**) the space occupied by the adamantyl moiety and by F331$^{6.58}$, viewed from the membrane plane. The $NTS_{8–13}$ complex is colored in green-cyan, the SR48692 complex in brown. Side chains are shown as sticks and are colored as the corresponding backbone. The isobutyl chain of Leu_{13} and the adamantyl moiety of SR48692 are shown as sticks and as van-der-Waals spheres, while the rest of the ligands as thin sticks. F331$^{6.58}$ is also shown as van-der-Waals spheres. TM4, ECL2, TM5, and TM7 have been omitted for clarity.

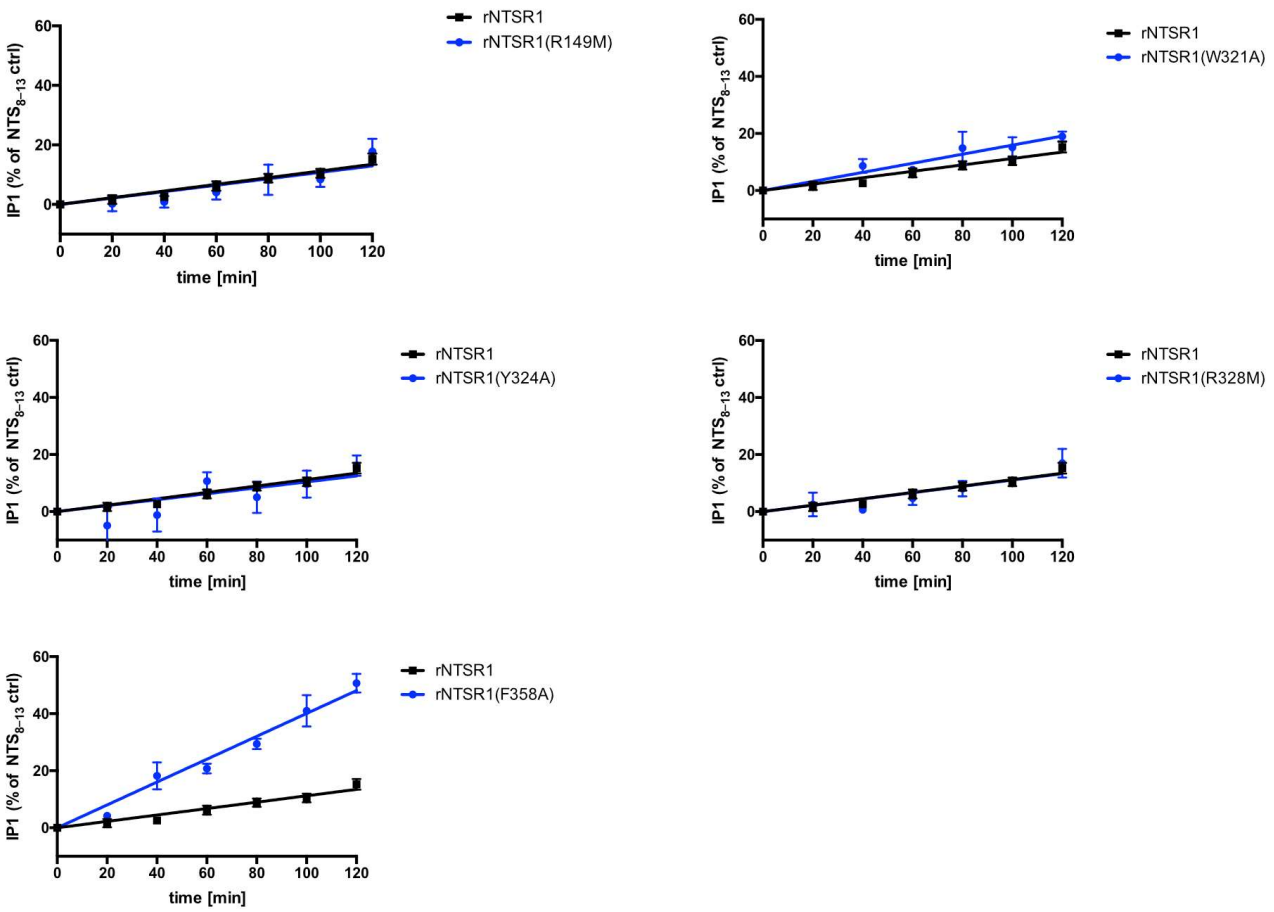

Fig. S16. Basal activity of rNTSR1 mutants compared to wild-type rNTSR1. Time-dependent IP1 accumulation measured in COS-7 cells transiently transfected with wild-type rNTSR1 or receptor mutants. To increase basal activity for IP1, all samples were co-transfected with $G\alpha_q$. Data were normalised to the IP1 response of the same receptor construct after stimulation with 10 µM $NTS_{8–13}$ for 120 min ($NTS_{8–13}$ ctrl). Data are shown as mean values ± SEM from 4–7 independent experiments performed in duplicates.

Supplementary tables

Table S1. Mutations of NTSR1-H4 compared to wild-type rNTSR1.

Sequential	B-W	wild-type rNTSR1	NTSR1-H4
83	1.51	S	G
86	1.54	A	L
101	2.38	T	R
103	2.40	H	D
105	2.42	H	Y
119	2.56	L	F
121	2.58	M	L
124	2.61	E	D
143	3.26	R	K
150	3.33	D	E
161	3.44	A	V
167	3.50	R	L
213	4.69	R	L
234	5.35	V	L
235	5.36	K	R
240	5.41	V	L
253	5.54	I	A
260	5.61	I	A
262	5.63	N	R
263	5.64	K	R
305	6.32	H	R
332	6.59	C	V
342	7.26	F	A
354	7.38	T	S
358	7.42	F	V
362	7.46	S	A

NTSR1-H4 has also been termed HTGH4 elsewhere (*9, 35*). In NTSR1-H4bm, the mutations E124$^{2.61}$D, D150$^{3.33}$E, F358$^{7.42}$V and S362$^{7.46}$A were reverted to the wild-type residues. B-W: Ballesteros-Weinstein numbering system.

Table S2. Competition ligand binding of HL488-NTS$_{8–13}$.

Construct	K_i (nM)				
	NTS$_{8–13}$	**SRI-9829**	**RTI-3a**	**SR48692**	**SR142948A**
rNTSR1	1.81 (1.31–2.50)	3227 (2002–5204)	183 (132–252)	19.6 (12.3–31.2)	1.98 (1.61–2.44)
NTSR1-H4$_X$	0.04 (0.03–0.06)	6.65 (4.29–10.3)	774 (470–1276)	736†† (493–1097)	39.5† (28.7–54.3)
NTSR1-H4$_X^{\Delta D12}$	0.05 (0.04–0.06)	6.48 (4.36–9.62)	730 (518–1027)	691†† (495–966)	27.3† (20.4–36.6)

Binding experiments were carried out on membranes from cells expressing rNTSR1 and the crystallized receptor variant with DARPin (NTSR1-H4$_X$) or without DARPin fusion (NTSR1-H4$_X^{\Delta D12}$) in the presence of different concentrations of unlabelled ligands as a competitor. Data are shown as mean values (95% CI in parentheses) from 5–9 independent experiments performed in duplicates.

†Direct K_D measurements by surface plasmon resonance (SPR) spectroscopy in detergent micelles indicated a higher affinity (~0.5 nM) (*66*), but the reasons for this discrepancy are currently unclear, leading to a possible underestimation of the affinity of SR142948A for NTSR1-H4 in competition experiments in cell membranes.

††A higher affinity (~87 nM) has been reported in detergent micelles when A647-NTS$_{8–13}$ was used as the tracer peptide (*34*), also suggesting that competition experiments in cell membranes might underestimate the affinity of SR48692 for NTSR1-H4.

Table S3. Data collection and refinement statistics of NTSR1-H4X structures.

Ligand	**NTS_{8-13}**	**SRI-9829**	**RTI-3a**	**SR48692**	**SR142948A**	**apo**
PDB code	**6YVR**	**6Z8N**	**6ZA8**	**6ZIN**	**6Z4Q**	**6Z66**
Data collection						
Space group	$P2_12_12_1$	$C222_1$	$C222_1$	C121	C121	$C222_1$
Cell dimensions						
a, b, c (Å)	89.89	76.67	76.47	212.98	211.92	76.19
	114.00	213.97	211.20	37.15	36.84	212.99
	195.42	94.05	93.70	91.21	90.29	94.64
α, β, γ (˚)	90	90	90	90	90	90
	90	90	90	113.60	113.65	90
	90	90	90	90	90	90
Resolution (Å)	29.62–2.46	29.58–2.80	29.62–2.72	28.57–2.64	28.31–2.92	29.44–3.19
	(2.65–2.46)	(3.13–2.80)	(3.01–2.72)	(2.97–2.64)	(3.32–2.92)	(3.44–3.19)
R_{merge}	0.094 (1.711)	0.208 (1.866)	0.259 (2.395)	0.123 (1.206)	0.202 (2.099)	0.33 (3.66)
R_{pim}	0.028 (0.555)	0.099 (0.820)	0.106 (0.913)	0.063 (0.612)	0.097 (0.895)	0.094 (1.034)
$I/\sigma(I)$	15.2 (1.6)	5.1 (1.4)	5.2 (1.6)	5.7 (1.2)	5.8 (1.5)	7.7 (1.3)
$CC_{1/2}$	0.999 (0.597)	0.982 (0.320)	0.975 (0.435)	0.993 (0.512)	0.989 (0.484)	0.993 (0.316)
Completeness (%)	93.9 (50.2)	90.4 (59.5)	90.4 (66.2)	85.4 (50.2)	78.2 (23.9)	91.6 (43.3)
Redundancy	12.0 (10.2)	5.2 (5.9)	6.5 (7.8)	4.5 (4.7)	4.7 (6.4)	13.3 (13.5)
Refinement						
Resolution (Å)	29.62–2.46	29.58–2.80	29.62–2.72	28.57–2.64	28.31–2.92	29.44–3.19
No. reflections	59974 (3000)	13189 (660)	13577 (679)	12018 (601)	8671 (434)	10818 (541)
Mol/ASU	2	1	1	1	1	1
R_{work}/R_{free}	0.228/0.237	0.270/0.301	0.281/0.304	0.272/0.315	0.281/0.307	0.286/0.294
No. atoms						
Protein	7001	3300	3352	3117	3025	3241
Ligand	131	34	37	41	50	-
Detergent	167	-	-	-	-	-
H_2O	47	-	-	-	-	-
R.m.s. deviations						
Bond lengths (Å)	0.01	0.01	0.01	0.01	0.01	0.01
Bond angles (˚)	1.67	1.64	1.64	1.68	1.67	1.67

Statistics were obtained from the STARANISO server (*61*) (see Methods). Mol/ASU: molecules per asymmetric unit. R.m.s.: root mean squared. Highest resolution shell is shown in parentheses.

Table S4. Data collection and refinement statistics of NTSR1-H4bmx structures.

Ligand	**$NTS_{8–13}$**	**SR48692**
PDB code	**6Z4V**	**6Z4S**
Data collection		
Space group	C121	$P2_12_12_1$
Cell dimensions		
a, b, c (Å)	69.22	43.52
	77.53	77.73
	111.86	158.39
α, β, γ (˚)	90	90
	107.22	90
	90	90
Resolution (Å)	29.23–2.60	29.34–2.71
	(2.80–2.60)	(3.03–2.71)
R_{merge}	0.453 (2.576)	0.525 (4.678)
R_{pim}	0.165 (0.970)	0.198 (1.504)
$I/\sigma(I)$	4.3 (1.5)	4.3 (1.4)
$CC_{1/2}$	0.921 (0.458)	0.964 (0.294)
Completeness (%)	88.9 (36.3)	90.6 (49.8)
Redundancy	8.5 (7.6)	7.3 (10.2)
Refinement		
Resolution (Å)	29.23–2.60	29.34–2.71
No. reflections	14177 (709)	10475 (524)
Mol/ASU	1	1
R_{work}/R_{free}	0.256/0.272	0.273/0.289
No. atoms		
Protein	3385	3286
Ligand	47	42
Detergent	-	-
H_2O	-	-
R.m.s. deviations		
Bond lengths (Å)	0.01	0.01
Bond angles (˚)	1.65	1.63

Statistics were obtained from the STARANISO server (*61*) (see Methods). Mol/ASU: molecules per asymmetric unit. R.m.s.: root mean squared. Highest resolution shell is shown in parentheses.

Table S5. Intermolecular interactions between $NTS_{8–13}$ and NTSR1-$H4_X$.

Ligand moiety	Interaction	NTSR1-$H4_X$ residue
Leu_{13} [O]	H, S	R327 [NH1; 2.5]
Leu_{13} [OXT]	H	Y146 [OH; 2.6]
Leu_{13} (isobutyl)	vdW	Y146, M204, M208, P227, L234†, I238, F331
Ile_{12} [amide O]	H	Y347 [OH; 2.6]
Ile_{12} (*sec*-butyl)	vdW	F128, H132, Y351
Tyr_{11} [amide O]	H	T226 [OG1; 2.7]
Tyr_{11} [amide N]	H	H348 [NE2; H_2O-mediated]
Tyr_{11} [OH]	H	L55 [amide O; 2.6]
Tyr_{11} [OH]	H	H132 [amide O; 3.4]
Tyr_{11} (phenyl)	vdW	L55, L213††, V224
Pro_{10} (pyrrolidine)	vdW	F331, W339, F344, Y347
Arg_9 [NE]	H	F331 [amide O, 3.4]
Arg_9 [NH1]	H, S	D336 [OD1; 2.6]
Arg_9 [NH2]	H	I334 [amide O; 2.1]
Arg_8 [NH2]	H	D56 [amide O; 3.0]
Arg_8 [NH2]	H	D54 [amide O; 2.6]
Arg_8 [NE]	Cation-π	F344 [ring center; 4.1]
Arg_8 [CZ]	Cation-π	F344 [ring center; 3.7]

For H-bonds (H) and salt bridges (S), the interacting atoms and their distance in Å are indicated in square brackets (cut-off: 3.6 Å; No angle terms were considered for H-bonds). Van-der-Waals interactions are abbreviated as vdW (cut-off: 4.5 Å). The term "aromatic interaction" is used as described in ref. (*67*). The analysis of cation-π interactions was based on Arpeggio, a web server for calculating and visualizing interatomic interactions in protein structures (http://biosig.unimelb.edu.au/arpeggioweb) (*68*).

†V234 in wild-type rNTSR1.

††R213 in wild-type rNTSR1.

Table S6. Intermolecular interactions between SRI-9829 and NTSR1-H4$_X$.

Ligand moiety	Interaction	NTSR1-H4$_X$ residue
Carboxyl [O3]	H, S	R327 [NH1; 2.8], R327 [NH2; 3.1]
Carboxyl [O4]	H	Y146 [OH; 2.6]
Isobutyl	vdW	Y146, M204, M208, I238, F331
Amide [N]	H	Y146 [OH; 3.2]
Amide [O]	H	Y347 [OH; 2.3]
Indole	vdW	F128, V131, F331, F344, Y347, H348, Y351
	Aromatic	F128, F331, F344, H348, Y351
Quinoline	vdW	V224, W339, F344
	Aromatic	W339, F344

For H-bonds (H) and salt bridges (S), the interacting atoms and their distance in Å are indicated in square brackets (cut-off: 3.6 Å; No angle terms were considered for H-bonds). Van-der-Waals interactions are abbreviated as vdW (cut-off: 4.5 Å). The term "aromatic interaction" is used as described in ref. (*67*). The analysis of aromatic interactions was based on Arpeggio, a web server for calculating and visualizing interatomic interactions in protein structures (http://biosig.unimelb.edu.au/arpeggioweb) (*68*).

Table S7. Intermolecular interactions between RTI-3a and NTSR1-H4$_X$.

Ligand moiety	Interaction	NTSR1-H4$_X$ residue
Carboxyl [O1]	H, S	R327 [NH1; 3.2], R327 [NH2; 3.2], R149 [NH1; 3.1]
Carboxyl [O2]	H, S	R149 [NH1; 3.6]
Carboxyl [O2]	H	Y146 [OH; 2.6]
Isobutyl	vdW	Y146, M204, M208, L234†, I238, F331
Amide [O]	H	R327 [NH1; 2.7], Y347 [OH; 2.6]
Pyrazole	vdW	F128, F331, Y347, Y351
	Aromatic	F128, F331, Y347, Y351
Dimethoxyphenyl	vdW	F128, V224, F331
Chloroquinoline	vdW	F128, H132, W339, F344, Y347, Y351
	Aromatic	H132, W339, Y347, Y351
	Halogen-π	H348

For H-bonds (H) and salt bridges (S), the interacting atoms and their distance in Å are indicated in square brackets (cut-off: 3.6 Å; No angle terms were considered for H-bonds). Van-der-Waals interactions are abbreviated as vdW (cut-off: 4.5 Å). The term "aromatic interaction" is used as described in ref. (*67*). The analysis of aromatic interactions was based on Arpeggio, a web server for calculating and visualizing interatomic interactions in protein structures (http://biosig.unimelb.edu.au/arpeggioweb) (*68*). Halogen-π interactions are defined as described in ref. (*69*).

†V234 in wild-type rNTSR1.

Table S8. Competition ligand binding of HL488-NTS$_{8–13}$ measured in cells expressing wild-type and rNTSR1 mutant constructs.

Construct	K_i (nM)		
	NTS$_{8–13}$	**SR48692**	**SR142948A**
rNTSR1	20.6 (15.3–27.7)	8.29 (6.63–10.4)	1.87 (0.85–4.10)
rNTSR1(R149M)	1.08 (0.6–1.95)		
rNTSR1(D150A)	16.3 (13.0–20.3)		
rNTSR1(V224A)	192.21 (99.6–371)		
rNTSR1(W321A)	1.38 (1.22–1.56)		
rNTSR1(Y324F)	13.3 (11.6–15.1)		
rNTSR1(R328M)	30.9 (17.2–55.4)		
rNTSR1(W339A)	150 (101–225)		
rNTSR1(F344A)	132 (64.3–272)		
rNTSR1(Y347F)	227 (154–333)	2.82 (1.77–4.47)	0.64 (0.38–1.07)
rNTSR1(H348A)	120.26 (67.7–214)		
rNTSR1(Y349A)	437 (108–1216)		
rNTSR1(Y351A)	1605.45 (1159.75–2222.44)		
rNTSR1(Y351F)	22.7 (17.53–29.4)		
rNTSR1(N355A)	34.3 (30.8–38.1)		
rNTSR1(F358A)	0.47 (0.37–0.61)		

Binding experiments were carried out on cells expressing wild-type and rNTSR1 mutant constructs in the presence of different concentrations of unlabelled ligands as a competitor.

Data are shown as mean values (95% CI in parentheses) from 3–9 independent experiments performed in duplicates.

Table S9. $NTS_{8–13}$-induced IP1 signalling measured in cells expressing wild-type and rNTSR1 mutant constructs.

Construct	EC_{50} (nM)
rNTSR1	2.08 (1.44–3.00)
rNTSR1(R149M)	1.82 (1.46–2.27)
rNTSR1(D150A)	10.2 (3.17–32.5)
rNTSR1(V224A)	327
rNTSR1(W321A)	0.60 (0.27–1.35)
rNTSR1(Y324F)	0.96 (0.46–2.00)
rNTSR1(R328M)	39.2 (22.6–67.9)
rNTSR1(W339A)	88.5 (57.0–137)
rNTSR1(F344A)	298 (139–639)
rNTSR1(Y347F)	494 (117–2077)
rNTSR1(H348A)	159 (67.8–374)
rNTSR1(Y349A)	492 (262–923)
rNTSR1(Y351A)	1156.11 (635.44–2103.4)
rNTSR1(Y351F)	1.36 (0.58–3.15)
rNTSR1(N355A)	7.55 (1.76–32.4)
rNTSR1(F358A)	0.32 (0.02–5.75)

Data are shown as mean values (95% CI in parentheses) from 3–10 independent experiments performed in duplicates.

Table S10. Intermolecular interactions between SR48692 and NTSR1-H4bm$_X$.

Ligand moiety	Interaction	NTSR1-H4bm$_X$ residue
Carboxyl [O1]	H, S	R327 [NH2; 2.4]
Carboxyl [O1]	H	Y351 [OH; 3.6]
Carboxyl [O2]	H, S	R328 [NH2; 3.0]
Adamantyl	vdW	Y146, M208, P227, L234[†], I238, F331
Pyrazole	vdW	F331, Y351
	Aromatic	F331, Y351
Dimethoxyphenyl	vdW	M330, F331, I334, Y347, F350
	Aromatic	Y347
Chloroquinoline	vdW	F331, F344, Y351
	Aromatic	Y351
	Halogen-π	F344

For H-bonds (H) and salt bridges (S), the interacting atoms and their distance in Å are indicated in square brackets (cut-off: 3.6 Å; No angle terms were considered for H-bonds). Van-der-Waals interactions are abbreviated as vdW (cut-off: 4.5 Å). The term "aromatic interaction" is used as described in ref. (*67*). The analysis of aromatic interactions was based on Arpeggio, a web server for calculating and visualizing interatomic interactions in protein structures (http://biosig.unimelb.edu.au/arpeggioweb) (*68*). Halogen-π interactions are defined as described in ref. (*69*).

[†]V234 in wild-type rNTSR1.

Table S11. Intermolecular interactions between SR142948A and NTSR1-H4$_X$.

Ligand moiety	Interaction	NTSR1-H4$_X$ residue
Carboxyl [O4]	H, S	R327 [NH2; 3.1]
Carboxyl [O4]	H	Y351 [OH; 2.6]
Carboxyl [O5]	H, S	R327 [NH2; 3.3], R328 [NH1; 3.5]
Adamantyl	vdW	Y146, M208, P227, L234†, I238
Pyrazole	vdW	Y351
	Aromatic	Y351
Dimethoxyphenyl	vdW	M330, I334, F350
Isopropylphenyl	vdW	Y351
	Aromatic	Y351

For H-bonds (H) and salt bridges (S), the interacting atoms and their distance in Å are indicated in square brackets (cut-off: 3.6 Å; No angle terms were considered for H-bonds). Van-der-Waals interactions are abbreviated as vdW (cut-off: 4.5 Å). The term "aromatic interaction" is used as described in ref. (*67*). The analysis of aromatic interactions was based on Arpeggio, a web server for calculating and visualizing interatomic interactions in protein structures (http://biosig.unimelb.edu.au/arpeggioweb) (*68*).

†V234 in wild-type rNTSR1.

Table S12. Crystallization conditions yielding optimized crystals of NTSR1-H4$_X$ and NTSR1-H4bm$_X$ in complex with different ligands or in the apo state.

Construct	Ligand	Condition	Method
NTSR1-H4$_X$	SRI-9829	100 mM HEPES pH 6.8, 370–520 mM Na citrate, 32% (v/v) PEG400, 10 µM SRI-9829	LCP
NTSR1-H4$_X$	RTI-3a	100 mM HEPES pH 6.6–7.2, 385–550 mM Na citrate, 30–32% (v/v) PEG400, 10 µM RTI-3a	LCP
NTSR1-H4$_X$	SR48692	100 mM Bis-Tris pH 6.4, 500 mM K citrate, 30% (v/v) PEG400	LCP
NTSR1-H4$_X$	SR142948A	100 mM Bis-Tris pH 6.5, 400 mM K citrate, 30% (v/v) PEG400, 10 µM SR142948A	LCP
NTSR1-H4$_X$	- (apo)	100 mM Na acetate pH 4.5, 400–475 mM K citrate, 30–31% (v/v) PEG400	LCP
NTSR1-H4bm$_X$	NTS$_{8–13}$	100 mM MES pH 6.2 and 6.3, 350–450 mM ammonium tartrate, 30% (v/v) PEG400	LCP
NTSR1-H4bm$_X$	SR48692	100 mM Na citrate pH 4.8–5.1, 225–460 mM ammonium nitrate, 30–32% (v/v) PEG400, 10 µM SR48692	LCP
NTSR1-H4$_X$	NTS$_{8–13}$	50 mM glycine pH 9.4, 1 M NaCl, 8.3% (w/v) PEG4000	VD

Crystallization in lipidic cubic phase and by vapor diffusion is abbreviated as LCP and VD, respectively.

Supplementary notes

Note S1

The binding mode of the carboxylate, adamantyl, amide, pyrazole and dimethoxyphenyl functional groups of SR48692 overlaps well with that of the corresponding groups of SR142948A (Fig. 4F). The binding mode of SR48692 as observed in the crystal structures (Fig. 4A, fig. S14, table S10) is consistent with the key role in ligand recognition previously assigned to a number of rNTSR1 residues by site-directed mutagenesis studies (*32*). R327$^{6.54}$ anchors the carboxylate group of SR48692 to the bottom of the binding site via ionic interactions, and R327$^{6.54}$M is devoid of SR48692 binding. Y351$^{7.35}$ forms polar interactions with the carboxylate group, and aromatic and van-der-Waals contacts with the pyrazole and chloroquinoline rings. Y351$^{7.35}$A causes a 200-fold drop in SR48692 affinity. M208$^{4.64}$ and F331$^{6.58}$ are part of the hydrophobic subpocket targeted by the adamantyl group. Furthermore, F331$^{6.58}$ forms aromatic interactions with the pyrazole ring. M208$^{4.64}$A and F331$^{6.58}$A lead to a 10- and 20-fold drop in affinity, respectively. The effect of F358$^{7.42}$A, a 5-fold decrease in affinity, can be likely explained by indirect conformational effects, as this mutation leads to constitutive activity (*19*) and thus preference for the active state. Y324$^{6.51}$ is positioned above F358$^{7.42}$ and below R327$^{6.54}$, and Y324$^{6.51}$A causes a 20-fold drop in affinity, likely by modulating the conformation of these residues. Y347$^{7.31}$F (table S8) causes a decrease in agonist affinity, compatible with H-bond formation (Fig. 3, A–C), but does not negatively affect inverse agonist binding, as no polar interaction is observed.

Supplementary materials and methods

Synthesis of SRI-9829 and SRI-9788

All solvents and chemicals were reagent grade, they were purchased from commercial vendors and used as received. Solvents used include acetonitrile, tetrahydrofuran (THF), hexane, ethyl acetate (EtOAc), dichloromethane (DCM), methanol and water. Flash column chromatography was carried out on a Teledyne ISCO CombiFlash Rf system using prepacked silica gel columns. Purity and characterization of compounds were established by a combination of HPLC, TLC, mass spectrometry, and NMR analyses. ^{1}H and ^{13}C NMR spectra were recorded on a Bruker AVANCE NEO (600 MHz) spectrometer or on a Bruker AVANCE DPX-400 (400 MHz) spectrometer, and were determined in d_6-DMSO or chloroform-d with solvent peaks as the internal reference. Chemical shifts are reported in ppm relative to the reference signal, and coupling constant (J) values are reported in Hertz (Hz). Mass spectra were obtained using a Thermo Scientific 1100 series/6120 Quadruple LC/MS (ESI). High resolution mass spectra (HRMS) were obtained using a Thermo Scientific EXACTIVE system (ESI).

(1-(quinolin-8-ylsulfonyl)-1H-indole-3-carbonyl)-L-leucine (SRI-9829). To a solution of methyl (1H-indole-3-carbonyl)-L-leucinate (45 mg, 0.156 mmol, CAS # 2714399-25-2) in THF (1 ml) was added NaH (60% dispersion in oil, 9.4 mg, 0.235 mmol, 1.5 eq) in one portion [methyl (1H-indole-3-carbonyl)-L-leucinate is available from Aurora Fine Chemicals, catalog # 191.857.980]. After stirring for 10 minutes, quinoline-8-sulfonyl chloride (43 mg, 0.189 mmol, 1.2 eq, CAS # 18704-37-5) was added, and the reaction was monitored by HPLC for disappearance of the starting material (quinoline-8-sulfonyl chloride is available from Oakwood Chemicals, catalog # 067922). After stirring at room temperature for 16 h, the reaction was quenched with water (0.5 ml). The crude reaction mixture was directly purified by reverse-phase preparative HPLC (CH_3CN/H_2O) to afford the title compound as a colorless solid. ^{1}H NMR (600 MHz, d_6-DMSO) δ 12.6 (broad s, 1H), 9.16 (s, 1H), 8.92 (dd, J =4.3 Hz, 1.8 Hz, 1H), 8.79 (dd, J = 7.4 Hz, 1.3 Hz, 1H), 8.74 (d, J = 8.0 Hz, 1H), 8.53 (dd, J = 8.4 Hz, 1.7 Hz, 1H), 8.44 (dd, J = 8.3 Hz, 1.3 Hz, 1H), 8.15–8.14 (m, 1H), 7.91 (dd, J =8.0 Hz, J =7.7 Hz, 1H), 7.76–7.74 (m, 1H), 7.69 (dd, J =8.3 Hz, 4.3 Hz, 1H), 7.29–7.23 (m, 2H), 4.54–4.51 (m,

1H), 1.88–1.81 (m, 2H), 1.7–1.66 (m, 1H), 1.03 (d, J = 6.5 Hz, 3H), 0.96 (d, J = 6.5 Hz, 3H); ^{13}C NMR (150 MHz, d_6-DMSO) 174.9, 163.6, 152.3, 143.1, 137.6, 136.9, 134.3, 133.6, 133.4, 132.8, 129.1, 128.8, 126.4, 125.0, 124.2, 123.6, 122.6, 113.8, 113.0, 50.7, 25.1, 23.4, 21.7; ESI-MS (m/z): 466.2 $[M+1]^+$.

Of note, related compounds analogous to SRI-9829 can also be synthesized by an alternate 3-step synthesis, which is more easily scaled up. As an example, we give the synthesis of (1-(naphthalen-1-ylsulfonyl)-1H-indole-3-carbonyl)-L-leucine (SRI-9788) here below.

Step 1: tert-butyl (1H-indole-3-carbonyl)-L-leucinate. To a mixture of 1H-indole-3-carboxylic acid (0.92 g, 5.7 mmol), tert-butyl L-leucinate hydrogen chloride (1.4 g, 6.3 mmol) and HATU (2.6 g, 6.8 mmol) in DCM (20 ml) was added diisopropylethylamine (3.0 ml, 17.1 mmol). The reaction was stirred at room temperature overnight. The mixture was concentrated *in vacuo* and the residue was dissolved with EtOAc, followed by washing with 1 N HCl, water, saturated aqueous $NaHCO_3$ and brine and dried over Na_2SO_4. The solvent was concentrated, and the crude was purified by silica gel flash chromatography to obtain the title compound. ^{1}H NMR (400 MHz, $CDCl_3$) δ 9.28 (broad s, 1H), 8.03 (dd, J = 8.0 Hz, 4.0 Hz, 1H), 7.76 (d, J = 3.0 Hz, 1H), 7.44–7.40 (m, 1H), 7.29–7.23 (m, 2H), 6.69 (d, J = 8.0 Hz, 1H), 4.89–4.83 (m, 1H), 1.87–1.74 (m, 3H), 1.52 (s, 9H), 1.04–0.95 (m, 6H); ^{13}C NMR (100 MHz, $CDCl_3$) 172.97, 165.03, 136.42, 128.46, 124.63, 122.83, 121.66, 119.85, 112.08, 111.93, 82.02, 51.37, 42.46, 28.06 (3C), 25.11, 22.90, 22.34; ESI-HRMS (m/z): 331.2022 $[M+1]^+$.

Step 2: tert-butyl (1-(naphthalen-1-ylsulfonyl)-1H-indole-3-carbonyl)-L-leucinate. To a mixture of tert-butyl (1H-indole-3-carbonyl)-L-leucinate (0.93 g, 2.83 mmol) in THF at 0°C was added NaH (60% in oil dispersion, 0.23 g, 5.7 mmol) portion wise. The mixture was allowed to warm to room temperature with stirring for 30 min and then re-cooled to 0°C in an ice bath. Naphthalene-1-sulfonyl chloride (0.84 g, 3.7 mmol) was added slowly and the mixture was allowed to warm to room temperature and stirred overnight. The reaction was quenched with saturated aqueous $NaHCO_3$ and extracted with EtOAc, washed with brine and dried over Na_2SO_4. The solvent was concentrated, and the crude was purified by silica gel flash chromatography to obtain the title compound. ^{1}H NMR (400 MHz, $CDCl_3$) δ 8.66 (d, J = 8.0 Hz, 1H), 8.30

(s, 1H), 8.22 (dd, J = 8.0 Hz, 4.0 Hz, 1H), 8.08 (d, J = 8.0 Hz, 1H), 8.04–8.00 (m, 1H), 7.88 (d, J = 8.0 Hz, 1H), 7.82–7.78 (m, 1H), 7.65 (td, J = 8.0 Hz, 4.0 Hz, 1H), 7.58–7.52 (m, 2H), 7.32–7.27 (m, 2H), 6.50–6.47 (m, 1H), 4.80–4.75 (m, 1H), 1.81–1.60 (m, 3H), 1.50 (s, 9H), 1.01–0.98 (m, 6H); ^{13}C NMR (100 MHz, $CDCl_3$) 172.41, 162.87, 136.13, 134.98, 134.25, 133.08, 129.94, 129.30, 129.20, 128.44, 128.01, 127.43, 127.28, 125.32, 124.26, 124.10, 123.59, 121.39, 116.72, 113.41, 82.24, 51.43, 42.32, 28.05 (3C), 25.10, 22.87, 22.34; ESI-HRMS (m/z): 521.2117 $[M+1]^+$.

Step 3: (1-(naphthalen-1-ylsulfonyl)-1H-indole-3-carbonyl)-L-leucine. Tert-butyl (1-(naphthalen-1-ylsulfonyl)-1H-indole-3-carbonyl)-L-leucinate (0.15 g) was dissolved in 30% TFA/DCM (1 ml) at room temperature. The reaction was monitored by reverse-phase analytical HPLC. When starting material was consumed, the reaction was diluted with MeOH and the solvent was removed *in vacuo* to obtain the title compound as a colorless solid. ^{1}H NMR (400 MHz, d_6-DMSO) δ 12.72 (broad s, 1H), 9.14 (s, 1H), 8.65 (t, J = 8.0 Hz, 2H), 8.58 (d, J = 8.0 Hz, 1H), 8.41 (d, J = 8.0 Hz, 1H), 8.20–8.15 (m, 2H), 7.83–7.70 (m, 4H), 7.36–7.28 (m, 2H), 4.53–4.48 (m, 1H), 1.84–1.64 (m, 3H), 1.01 (d, J = 4.0 Hz, 3H), 0.93 (d, J = 8.0 Hz, 3H); ^{13}C NMR (100 MHz, d_6-DMSO) 174.22, 162.59, 136.77, 133.80, 133.66, 131.31, 131.09, 129.73, 129.21, 129.09, 128.22, 127.58, 126.80, 125.18, 124.83, 124.05, 122.83, 122.37, 114.94, 112.56, 50.27, 24.51, 22.88, 21.26 (2C); ESI-HRMS (m/z): 465.1477 $[M+1]^+$.

REFERENCES AND NOTES

1. J. P. Vincent, J. Mazella, P. Kitabgi, Neurotensin and neurotensin receptors. *Trends Pharmacol. Sci.* **20**, 302–309 (1999).

2. B. Holst, N. D. Holliday, A. Bach, C. E. Elling, H. M. Cox, T. W. Schwartz, Common structural basis for constitutive activity of the ghrelin receptor family. *J. Biol. Chem.* **279**, 53806–53817 (2004).

3. K. Sriram, P. A. Insel, G protein-coupled receptors as targets for approved drugs: How many targets and how many drugs? *Mol. Pharmacol.* **93**, 251–258 (2018).

4. D. S. Wishart, Y. D. Feunang, A. C. Guo, E. J. Lo, A. Marcu, J. R. Grant, T. Sajed, D. Johnson, C. Li, Z. Sayeeda, N. Assempour, I. Iynkkaran, Y. Liu, A. Maciejewski, N. Gale, A. Wilson, L. Chin, R. Cummings, D. Le, A. Pon, C. Knox, M. Wilson, DrugBank 5.0: A major update to the DrugBank database for 2018. *Nucleic Acids Res.* **46**, D1074–D1082 (2018).

5. J. A. Henry, D. C. Horwell, K. G. Meecham, D. C. Rees, A structure-affinity study of the amino acid side-chains in neurotensin: N and C terminal deletions and Ala-scan. *Bioorg. Med. Chem. Lett.* **3**, 949–952 (1993).

6. C. Granier, J. van Rietschoten, P. Kitabgi, C. Poustis, P. Freychet, Synthesis and characterization of neurotensin analogues for structure/activity relationship studies. Acetyl-neurotensin-(8–13) is the shortest analogue with full binding and pharmacological activities. *Eur. J. Biochem.* **124**, 117–124 (1982).

7. É. Besserer-Offroy, R. L. Brouillette, S. Lavenus, U. Froehlich, A. Brumwell, A. Murza, J.-M. Longpré, É. Marsault, M. Grandbois, P. Sarret, R. Leduc, The signaling signature of the neurotensin type 1 receptor with endogenous ligands. *Eur. J. Pharmacol.* **805**, 1–13 (2017).

8. J. F. White, N. Noinaj, Y. Shibata, J. Love, B. Kloss, F. Xu, J. Gvozdenovic-Jeremic, P. Shah, J. Shiloach, C. G. Tate, R. Grisshammer, Structure of the agonist-bound neurotensin receptor. *Nature* **490**, 508–513 (2012).

9. P. Egloff, M. Hillenbrand, C. Klenk, A. Batyuk, P. Heine, S. Balada, K. M. Schlinkmann, D. J. Scott, M. Schütz, A. Plückthun, Structure of signaling-competent neurotensin receptor 1 obtained by directed evolution in *Escherichia coli*. *Proc. Natl. Acad. Sci. U.S.A.* **111**, E655–E662 (2014).

10. B. E. Krumm, J. F. White, P. Shah, R. Grisshammer, Structural prerequisites for G-protein activation by the neurotensin receptor. *Nat. Commun.* **6**, 7895 (2015).

11. B. E. Krumm, S. Lee, S. Bhattacharya, I. Botos, C. F. White, H. Du, N. Vaidehi, R. Grisshammer, Structure and dynamics of a constitutively active neurotensin receptor. *Sci. Rep.* **6**, 38564 (2016).

12. H. E. Kato, Y. Zhang, H. Hu, C.-M. Suomivuori, F. M. N. Kadji, J. Aoki, K. Krishna Kumar, R. Fonseca, D. Hilger, W. Huang, N. R. Latorraca, A. Inoue, R. O. Dror, B. K. Kobilka, G. Skiniotis, Conformational transitions of a neurotensin receptor 1-G_{i1} complex. *Nature* **572**, 80–85 (2019).

13. D. Gully, M. Canton, R. Boigegrain, F. Jeanjean, J. C. Molimard, M. Poncelet, C. Gueudet, M. Heaulme, R. Leyris, A. Brouard, Biochemical and pharmacological profile of a potent and selective nonpeptide antagonist of the neurotensin receptor. *Proc. Natl. Acad. Sci. U.S.A.* **90**, 65–69 (1993).

14. D. Gully, B. Labeeuw, R. Boigegrain, F. Oury-Donat, A. Bachy, M. Poncelet, R. Steinberg, M. F. Suaud-Chagny, V. Santucci, N. Vita, F. Pecceu, C. Labbé-Jullié, P. Kitabgi, P. Soubrié, G. Le Fur, J. P. Maffrand, Biochemical and pharmacological activities of SR 142948A, a new potent neurotensin receptor antagonist. *J. Pharmacol. Exp. Ther.* **280**, 802–812 (1997).

15. R. E. Carraway, A. M. Plona, Involvement of neurotensin in cancer growth: Evidence, mechanisms and development of diagnostic tools. *Peptides* **27**, 2445–2460 (2006).

16. Z. Wu, D. Martinez-Fong, J. Trédaniel, P. Forgez, Neurotensin and its high affinity receptor 1 as a potential pharmacological target in cancer therapy. *Front. Endocrinol. (Lausanne)* **3**, 184 (2013).

17. Q. Ouyang, J. Zhou, W. Yang, H. Cui, M. Xu, L. Yi, Oncogenic role of neurotensin and neurotensin receptors in various cancers. *Clin. Exp. Pharmacol. Physiol.* **44**, 841–846 (2017).

18. J. Liu, M. Agopiantz, J. Poupon, Z. R. Wu, P.-A. Just, B. Borghese, E. Ségal-Bendirdjian, G. Gauchotte, A. Gompel, P. Forgez, Neurotensin receptor 1 antagonist SR48692 improves response to

carboplatin by enhancing apoptosis and inhibiting drug efflux in ovarian cancer. *Clin. Cancer Res.* **23**, 6516–6528 (2017).

19. S. Barroso, F. Richard, D. Nicolas-Ethève, P. Kitabgi, C. Labbé-Jullié, Constitutive activation of the neurotensin receptor 1 by mutation of Phe(358) in helix seven. *Br. J. Pharmacol.* **135**, 997–1002 (2002).

20. R. C. Kling, M. Plomer, C. Lang, A. Banerjee, H. Hübner, P. Gmeiner, Development of covalent ligand-receptor pairs to study the binding properties of nonpeptidic neurotensin receptor 1 antagonists. *ACS Chem. Biol.* **11**, 869–875 (2016).

21. J. B. Thomas, H. Navarro, K. R. Warner, B. Gilmour, The identification of nonpeptide neurotensin receptor partial agonists from the potent antagonist SR48692 using a calcium mobilization assay. *Bioorg. Med. Chem. Lett.* **19**, 1438–1441 (2009).

22. P. Di Fruscia, Y. He, M. Koenig, S. Tabrizifard, A. Nieto, P. H. McDonald, T. M. Kamenecka, The discovery of indole full agonists of the neurotensin receptor 1 (NTSR1). *Bioorg. Med. Chem. Lett.* **24**, 3974–3978 (2014).

23. F. St-Gelais, C. Jomphe, L.-E. Trudeau, The role of neurotensin in central nervous system pathophysiology: What is the evidence? *J. Psychiatry Neurosci.* **31**, 229–245 (2006).

24. M. Boules, Z. Li, K. Smith, P. Fredrickson, E. Richelson, Diverse roles of neurotensin agonists in the central nervous system. *Front. Endocrinol.* **4**, 36 (2013).

25. W. C. Mustain, P. G. Rychahou, B. M. Evers, The role of neurotensin in physiologic and pathologic processes. *Curr. Opin. Endocrinol. Diabetes Obes.* **18**, 75–82 (2011).

26. O. Osadchii, A. Woodiwiss, G. Norton, *Neuropeptide Research Trends Ch. 1* (Nova Science Publishers, 2007), pp. 13–63.

27. K. Kalafatakis, K. Triantafyllou, Contribution of neurotensin in the immune and neuroendocrine modulation of normal and abnormal enteric function. *Regul. Pept.* **170**, 7–17 (2011).

28. J. Li, J. Song, Y. Y. Zaytseva, Y. Liu, P. Rychahou, K. Jiang, M. E. Starr, J. T. Kim, J. W. Harris, F. B. Yiannikouris, W. S. Katz, P. M. Nilsson, M. Orho-Melander, J. Chen, H. Zhu, T. Fahrenholz, R. M. Higashi, T. Gao, A. J. Morris, L. A. Cassis, T. W.-M. Fan, H. L. Weiss, P. R. Dobner, O. Melander, J. Jia, B. M. Evers, An obligatory role for neurotensin in high-fat-diet-induced obesity. *Nature* **533**, 411–415 (2016).

29. O. E. Osadchii, Emerging role of neurotensin in regulation of the cardiovascular system. *Eur. J. Pharmacol.* **762**, 184–192 (2015).

30. A. M. Piliponsky, C.-C. Chen, T. Nishimura, M. Metz, E. J. Rios, P. R. Dobner, E. Wada, K. Wada, S. Zacharias, U. M. Mohanasundaram, J. D. Faix, M. Abrink, G. Pejler, R. G. Pearl, M. Tsai, S. J. Galli, Neurotensin increases mortality and mast cells reduce neurotensin levels in a mouse model of sepsis. *Nat. Med.* **14**, 392–398 (2008).

31. B. M. Evers, Neurotensin and growth of normal and neoplastic tissues. *Peptides* **27**, 2424–2433 (2006).

32. C. Labbé-Jullié, S. Barroso, D. Nicolas-Etève, J. L. Reversat, J. M. Botto, J. Mazella, J. M. Bernassau, P. Kitabgi, Mutagenesis and modeling of the neurotensin receptor NTR1. Identification of residues that are critical for binding SR 48692, a nonpeptide neurotensin antagonist. *J. Biol. Chem.* **273**, 16351–16357 (1998).

33. M. Lückmann, B. Holst, T. W. Schwartz, T. M. Frimurer, In silico investigation of the neurotensin receptor 1 binding site: Overlapping binding modes for small molecule antagonists and the endogenous peptide agonist. *Mol. Inform.* **35**, 19–24 (2016).

34. D. J. Scott, L. Kummer, P. Egloff, R. A. D. Bathgate, A. Plückthun, Improving the apo-state detergent stability of NTS_1 with CHESS for pharmacological and structural studies. *Biochim. Biophys. Acta* **1838**, 2817–2824 (2014).

35. P. Egloff, M. Deluigi, P. Heine, S. Balada, A. Plückthun, A cleavable ligand column for the rapid isolation of large quantities of homogeneous and functional neurotensin receptor 1 variants from *E. coli*. *Protein Expr. Purif.* **108**, 106–114 (2015).

36. P. Heine, G. Witt, A. Gilardi, P. Gribbon, L. Kummer, A. Plückthun, High-throughput fluorescence polarization assay to identify ligands using purified G protein-coupled receptor. *SLAS Discov.* **24**, 915–927 (2019).

37. A. Ranganathan, P. Heine, A. Rudling, A. Plückthun, L. Kummer, J. Carlsson, Ligand discovery for a peptide-binding GPCR by structure-based screening of fragment- and lead-like chemical libraries. *ACS Chem. Biol.* **12**, 735–745 (2017).

38. E. Chun, A. A. Thompson, W. Liu, C. B. Roth, M. T. Griffith, V. Katritch, J. Kunken, F. Xu, V. Cherezov, M. A. Hanson, R. C. Stevens, Fusion partner toolchest for the stabilization and crystallization of G protein-coupled receptors. *Structure* **20**, 967–976 (2012).

39. Y. Wu, A. Batyuk, A. Honegger, F. Brandl, P. R. E. Mittl, A. Plückthun, Rigidly connected multispecific artificial binders with adjustable geometries. *Sci. Rep.* **7**, 11217 (2017).

40. P. Ernst, A. Honegger, F. van der Valk, C. Ewald, P. R. E. Mittl, A. Plückthun, Rigid fusions of designed helical repeat binding proteins efficiently protect a binding surface from crystal contacts. *Sci. Rep.* **9**, 16162 (2019).

41. P. R. E. Mittl, P. Ernst, A. Plückthun, Chaperone-assisted structure elucidation with DARPins. *Curr. Opin. Struct. Biol.* **60**, 93–100 (2020).

42. F. Bumbak, A. C. Keen, N. J. Gunn, P. R. Gooley, R. A. D. Bathgate, D. J. Scott, Optimization and $^{13}CH_3$ methionine labeling of a signaling competent neurotensin receptor 1 variant for NMR studies. *Biochim. Biophys. Acta* **1860**, 1372–1383 (2018).

43. T. Warne, P. C. Edwards, A. S. Doré, A. G. W. Leslie, C. G. Tate, Molecular basis for high-affinity agonist binding in GPCRs. *Science* **364**, 775–778 (2019).

44. T. Che, S. Majumdar, S. A. Zaidi, P. Ondachi, J. D. McCorvy, S. Wang, P. D. Mosier, R. Uprety, E. Vardy, B. E. Krumm, G. W. Han, M.-Y. Lee, E. Pardon, J. Steyaert, X.-P. Huang, R. T. Strachan, A. R. Tribo, G. W. Pasternak, F. I. Carroll, R. C. Stevens, V. Cherezov, V. Katritch, D. Wacker, B. L. Roth, Structure of the nanobody-stabilized active state of the kappa opioid receptor. *Cell* **172**, 55–67.e15 (2018).

45. S. Nagarajan, N. J. Alkayed, S. Kaul, A. P. Barnes, Effect of thermostable mutations on the neurotensin receptor 1 (NTSR1) activation state. *J. Biomol. Struct. Dyn.* **38**, 340–353 (2020).

46. P. Kitabgi, C. Poustis, C. Granier, J. van Rietschoten, J. Rivier, J.-L. Morgat, P. Freychet, Neurotensin binding to extraneural and neural receptors: Comparison with biological activity and structure—Activity-relationships. *Mol. Pharmacol.* **18**, 11–19 (1980).

47. F. Bumbak, T. Thomas, B. J. Noonan-Williams, T. M. Vaid, F. Yan, A. R. Whitehead, S. Bruell, M. Kocan, X. Tan, M. A. Johnson, R. A. D. Bathgate, D. K. Chalmers, P. R. Gooley, D. J. Scott, Conformational changes in tyrosine 11 of neurotensin are required to activate the neurotensin receptor 1. *ACS Pharmacol. Transl. Sci.* **3**, 690–705 (2020).

48. P. M. Hershberger, M. P. Hedrick, S. Peddibhotla, A. Mangravita-Novo, P. Gosalia, Y. Li, W. Gray, M. Vicchiarelli, L. H. Smith, T. D. Y. Chung, J. B. Thomas, M. G. Caron, A. B. Pinkerton, L. S. Barak, G. P. Roth, Imidazole-derived agonists for the neurotensin 1 receptor. *Bioorg. Med. Chem. Lett.* **24**, 262–267 (2014).

49. F. Richard, S. Barroso, D. Nicolas-Ethève, P. Kitabgi, C. Labbé-Jullié, Impaired G protein coupling of the neurotensin receptor 1 by mutations in extracellular loop 3. *Eur. J. Pharmacol.* **433**, 63–71 (2001).

50. I. Goba, D. Goricanec, D. Schum, M. Hillenbrand, A. Plückthun, F. Hagn, Probing the conformation states of neurotensin receptor 1 variants by NMR site-directed methyl labeling. *Chembiochem*, in press (2020).

51. V. Katritch, V. Cherezov, R. C. Stevens, Structure-function of the G protein-coupled receptor superfamily. *Annu. Rev. Pharmacol. Toxicol.* **53**, 531–556 (2013).

52. W. I. Weis, B. K. Kobilka, The molecular basis of G protein-coupled receptor activation. *Annu. Rev. Biochem.* **87**, 897–919 (2018).

53. V. Katritch, G. Fenalti, E. E. Abola, B. L. Roth, V. Cherezov, R. C. Stevens, Allosteric sodium in class A GPCR signaling. *Trends Biochem. Sci.* **39**, 233–244 (2014).

54. W. Shihoya, T. Izume, A. Inoue, K. Yamashita, F. M. N. Kadji, K. Hirata, J. Aoki, T. Nishizawa, O. Nureki, Crystal structures of human ET_B receptor provide mechanistic insight into receptor activation and partial activation. *Nat. Commun.* **9**, 4711 (2018).

55. F. Wu, G. Song, C. de Graaf, R. C. Stevens, Structure and function of peptide-binding G protein-coupled receptors. *J. Mol. Biol.* **429**, 2726–2745 (2017).

56. S. M. Advani, P. G. Advani, H. M. VonVille, S. H. Jafri, Pharmacological management of cachexia in adult cancer patients: A systematic review of clinical trials. *BMC Cancer* **18**, 1174 (2018).

57. J. Schulz, M. Rohracker, M. Stiebler, J. Goldschmidt, F. Stöber, M. Noriega, A. Pethe, M. Lukas, F. Osterkamp, U. Reineke, A. Höhne, C. Smerling, H. Amthauer, Proof of therapeutic efficacy of a ^{177}Lu-labeled neurotensin receptor 1 antagonist in a colon carcinoma xenograft model. *J. Nucl. Med.* **58**, 936–941 (2017).

58. R. P. Baum, A. Singh, C. Schuchardt, H. R. Kulkarni, I. Klette, S. Wiessalla, F. Osterkamp, U. Reineke, C. Smerling, ^{177}Lu-3BP-227 for neurotensin receptor 1-targeted therapy of metastatic pancreatic adenocarcinoma: First clinical results. *J. Nucl. Med.* **59**, 809–814 (2018).

59. N. R. Latorraca, A. J. Venkatakrishnan, R. O. Dror, GPCR dynamics: Structures in motion. *Chem. Rev.* **117**, 139–155 (2017).

60. S. Basu, J. W. Kaminski, E. Panepucci, C. Y. Huang, R. Warshamanage, M. Wang, J. A. Wojdyla, Automated data collection and real-time data analysis suite for serial synchrotron crystallography. *J. Synchrotron Radiat.* **26**, 244–252 (2019).

61. I. J. Tickle, C. Flensburg, P. Keller, W. Paciorek, A. Sharff, C. Vonrhein, G. Bricogne, STARANISO (2018); http://staraniso.globalphasing.org.

62. J. D. Durrant, L. Votapka, J. Sørensen, R. E. Amaro, POVME 2.0: An enhanced tool for determining pocket shape and volume characteristics. *J. Chem. Theory Comput.* **10**, 5047–5056 (2014).

63. C. Klenk, T. Vetter, A. Zürn, J.-P. Vilardaga, P. A. Friedman, B. Wang, M. J. Lohse, Formation of a ternary complex among NHERF1, β-arrestin, and parathyroid hormone receptor. *J. Biol. Chem.* **285**, 30355–30362 (2010).

64. Y.-C. Cheng, W. H. Prusoff, Relationship between the inhibition constant (K_i) and the concentration of inhibitor which causes 50 per cent inhibition (I_{50}) of an enzymatic reaction. *Biochem. Pharmacol.* **22**, 3099–3108 (1973).

65. J. Ehrenmann, J. Schöppe, C. Klenk, M. Rappas, L. Kummer, A. S. Doré, A. Plückthun, High-resolution crystal structure of parathyroid hormone 1 receptor in complex with a peptide agonist. *Nat. Struct. Mol. Biol.* **25**, 1086–1092 (2018).

66. S. Huber, F. Casagrande, M. N. Hug, L. S. Wang, P. Heine, L. Kummer, A. Plückthun, M. Hennig, SPR-based fragment screening with neurotensin receptor 1 generates novel small molecule ligands. *PLOS ONE* **12**, e0175842 (2017).

67. C. R. Martinez, B. L. Iverson, Rethinking the term "pi-stacking". *Chem. Sci.* **3**, 2191–2201 (2012).

68. H. C. Jubb, A. P. Higueruelo, B. Ochoa-Montaño, W. R. Pitt, D. B. Ascher, T. L. Blundell, Arpeggio: A web server for calculating and visualising interatomic interactions in protein structures. *J. Mol. Biol.* **429**, 365–371 (2017).

69. Y. N. Imai, Y. Inoue, I. Nakanishi, K. Kitaura, Cl-π interactions in protein-ligand complexes. *Protein Sci.* **17**, 1129–1137 (2008).